

# Design Automation for Microfluidics-Based Biochips

KRISHNENDU CHAKRABARTY

Duke University

and

JUN ZENG

Coventor, Inc.

---

Advances in microfluidics technology offer exciting possibilities in the realm of enzymatic analysis, DNA analysis, proteomic analysis involving proteins and peptides, immunoassays, implantable drug delivery devices, and environmental toxicity monitoring. Microfluidics-based biochips are therefore gaining popularity for clinical diagnostics and other laboratory procedures involving molecular biology. As more bioassays are executed concurrently on a biochip, system integration and design complexity are expected to increase dramatically. This paper presents different actuation mechanisms for microfluidics-based biochips, as well as associated design automation trends and challenges. The underlying physical principles of electrokinetics, electrohydrodynamics, and thermocapillarity are discussed. Next, the paper presents an overview of an integrated system-level design methodology that attempts to address key issues in the modeling, simulation, synthesis, testing and reconfiguration of digital microfluidics-based biochips. The top-down design automation will facilitate the integration of fluidic components with microelectronic component in next-generation system-on-chip designs.

Categories and Subject Descriptors: B.m [**Miscellaneous**]: *Design management*

General Terms: Algorithms, Design, Performance, Reliability

Additional Key Words and Phrases: Microfluidics, biochips, design automation

---

This article is an extended version of the paper that has appeared in *Proceedings of the IEEE Conference on Nanotechnology*, IEEE Computer Society Press, Los Alamitos, CA, 2005.

The work of K. Chakrabarty was supported in part by the National Science Foundation (NSF) under grant number IIS-0312352.

Coventor's simulation projects were supported in part by the Defense Advanced Research Projects Agency Composite CAD program (grants F30602-98-2-0151 and F30602-96-2-0306), and BioFlips program (contract DAAD10-00-1-0515 from the Army Research Office to the University of Texas M. D. Anderson Cancer Center).

Authors' addresses: K. Chakrabarty, Department of Electrical and Computer Engineering, Duke University, Durham, NC 27708; email: krish@ee.duke.edu; J. Zeng, Coventor, Inc., 625 Mount Auburn Street, Cambridge, MA 02138; email: jzeng@coventor.com.

Permission to make digital or hard copies of part or all of this work for personal or classroom use is granted without fee provided that copies are not made or distributed for profit or direct commercial advantage and that copies show this notice on the first page or initial screen of a display along with the full citation. Copyrights for components of this work owned by others than ACM must be honored. Abstracting with credit is permitted. To copy otherwise, to republish, to post on servers, to redistribute to lists, or to use any component of this work in other works requires prior specific permission and/or a fee. Permissions may be requested from Publications Dept., ACM, Inc., 1515 Broadway, New York, NY 10036 USA, fax: +1 (212) 869-0481, or permissions@acm.org.

© 2005 ACM 1550-4832/05/1000-0186 \$5.00

## 1. INTRODUCTION

Microfluidics-based biochips are soon expected to revolutionize laboratory procedures involving molecular biology [Burns et al. 1998; Zhang et al. 2002; Thorsen et al. 2002; Verpoorte and De Rooij 2003]. These composite microsystems, also known as *lab-on-a-chip* or *bio-MEMS*, automate highly repetitive laboratory tasks by replacing cumbersome equipment with miniaturized and integrated systems, and they enable the handling of small amounts, for example, micro- and nanoliters, of fluids. Thus, compared to traditional methods, they are able to provide ultrasensitive detection at significantly lower cost and much faster speed.

Advances in microfluidics technology offer exciting possibilities in the realm of enzymatic analysis (e.g., glucose and lactate assays), DNA analysis (e.g., PCR and nucleic acid sequence analysis), proteomic analysis [Lion et al. 2003] involving proteins and peptides, immuno-assays, implantable drug delivery devices [Grayson et al. 2004], and environmental toxicity monitoring. An emerging application area for microfluidics-based biochips is clinical diagnostics, especially immediate point-of-care diagnosis of diseases [Schulte et al. 2002; Srinivasan et al. 2004]. Microfluidics-based devices, capable of continuous sampling and real-time testing of air/water samples for biochemical toxins and other dangerous pathogens, can serve as an always-on “bio-smoke alarm” for early warning [Hull et al. 2003; Venkatesh and Memish 2003].

The first generation of microfluidic biochips contained permanently etched micro-pumps, micro-valves, and micro-channels, and their operation was based on the principle of continuous fluid flow [Thorsen et al. 2002; Verpoorte and De Rooij 2003]. A promising alternative is to manipulate liquids as discrete droplets [Pollack et al. 2000; Cho et al. 2002]. Following the analogy of micro-electronics, this approach is referred to as “digital microfluidics”. In contrast to continuous-flow biochips, digital microfluidics-based biochips offer a scalable system architecture based on a two-dimensional microfluidic array of identical basic unit cells. Moreover, because each droplet can be controlled independently, these systems also have dynamic reconfigurability, whereby groups of unit cells in a microfluidic array can be reconfigured to change their functionality during the concurrent execution of a set of bioassays.

As the use of microfluidics-based biochips increases, their complexity is expected to become significant due to the need for multiple and concurrent assays on the chip. There is a need to deliver the same level of computer-aided design (CAD) support to the biochip designer that the semiconductor industry now takes for granted. These CAD tools will allow designers to harness the new technology that is rapidly emerging for integrated microfluidics. They will also provide the means to advance the state-of-the-art from the design of application-specific biochips to the design of general-purpose, programmable, and miniaturized analytical systems. Current design practices that rely on back-of-the-envelope calculations are not only inefficient, but they are also not rigorous enough to meet mandated system specifications.

The 2003 International Technology Roadmap for Semiconductors (ITRS) clearly identifies the integration of electrochemical and electro-biological

techniques as one of the system-level design challenges that will be faced beyond 2009, when feature sizes shrink below 50 nm [ITRS 2003]. Efforts are underway in the CAD community to identify synergies between biochips and microelectronics CAD. The 2005 *Design, Automation, and Test in Europe (DATE) Conference* included a well-attended “Biochips Day” event. The *IEEE Transactions on CAD/ICAS* will publish a special issue on biochips in February 2006. A special session on bioMEMS was organized at the 2004 *IEEE/ACM Design Automation Conference*. A full-day workshop on emerging CAD issues for biochips will be included as part of the technical program for *DATE* 2006.

Reliability is an important performance parameter for microfluidics-based biochips that are used in safety-critical applications. These systems need to be tested adequately not only after fabrication, but also continuously during field operation. For instance, for detectors monitoring the environment for dangerous pathogens in critical locations such as airports, field-testing is critical to ensure low false-positive and false-negative detection rates. The ITRS 2003 document recognizes the need for new test methods for disruptive device technologies that underly microelectromechanical systems and sensors, and highlights it as one of the five difficult test challenges beyond 2009 [ITRS 2003].

The reconfigurability inherent in digital microfluidic biochips can be utilized to achieve longer system lifetimes through on-line reconfiguration to avoid operational faults. It can also be used to increase production yield through production-time reconfiguration to bypass manufacturing faults. The configuration of the microfluidic array must therefore be changed in such a way that the functionality of the bioassays is not compromised.

In this article, we describe an integrated methodology for modeling, simulation, synthesis, testing and reconfiguration of microfluidic-based biochips. We show how top-down system-level design automation tools can relieve biochip users from the burden of manual optimization of assays, time-consuming hardware design, and costly testing and maintenance procedures. Users will be able to describe bioassays at a sufficiently high level of abstraction. Device simulation tools will be used for design validation of individual components and to characterize component libraries. System simulation and synthesis tools will map the behavioral description to a microfluidic biochip and generate an optimized schedule of bioassay operations, the binding of assay operations to resources, and a layout of the microfluidic biochip. For fabricated microfluidic biochips, cost-effective testing techniques will be available to detect faulty unit cells after manufacture and during field operation. Online and offline reconfiguration techniques, incorporated in these design automation tools, will be used to easily bypass faults once they are detected. The methodology and tools for top-down design will reduce human effort and enable high-volume production. Equipped with a top-down design environment, the biochip designer can concentrate on the development of the nano- and micro-scale bioassays, leaving implementation details to the design automation tools.

The remainder of the article is organized as follows. Section 2 presents an overview of microfluidic technologies and CAD tools for microfluidics-based biochips. Section 3 describes a new automated top-down design flow. Section 4

presents device simulation methods for microfluidics. In Section 5, we describe how system simulation can be carried out for microfluidic biochips. Section 6 describes synthesis, testing, and reconfiguration techniques. Finally, Section 7 concludes the article and outlines directions for future research.

## 2. STATE-OF-THE-ART IN MICROFLUIDIC TECHNOLOGIES AND COMPUTER-AIDED DESIGN METHODS

In this section, we review currently available microfluidic technologies and the state-of-the-art in CAD tools for the design of microfluidics-based systems.

### 2.1 Technology Overview

Early biochips were based on the concept of a DNA microarray, which is a piece of glass, plastic or silicon substrate on which pieces of DNA have been affixed in a microscopic array. The affixed DNA segments are known as probes. There are a number of commercial microarrays available in the marketplace today, for example, the GeneChip® DNAarray from Affymetrix, the DNA microarray from Infineon AG, and the NanoChip® microarray from Nanogen [Affymetrix GeneChip, Infineon, Nanogen]. Similar to a DNA microarray, a protein array is a miniature array where a multitude of different capture agents, most frequently monoclonal antibodies, are deposited on a chip surface (glass or silicon); they are used to determine the presence and/or amount of proteins in biological samples, for example, blood. A drawback of DNA and protein arrays is that they are neither reconfigurable nor scalable after manufacture.

The basic idea of microfluidic biochips is to integrate all necessary functions for biochemical analysis onto one chip using microfluidics technology. These micro-total-analysis-systems ( $\mu$ TAS) are more versatile and complex than microarrays. Integrated functions include microfluidic assay operations and detection, as well as sample pre-treatment and preparation. The first generation of microfluidic biochips contained permanently etched structures such as pumps, valves and channels, and relied on continuous liquid flow stream to carry out specific tasks. This type of biochips hereafter is referred to as *continuous-flow microfluidics* or *channel-based* biochips. On the contrary, *digital microfluidics*, the second-generation biochip architecture, relies on discrete liquid particles to carry out general-purpose analysis.

**2.1.1 Continuous-Flow Microfluidics.** These technologies are based on the manipulation of continuous liquid flow through micro-fabricated channels. Actuation of liquid flow is implemented either by external pressure sources, integrated mechanical micro-pumps, or by electrokinetic mechanisms [Thorsen et al. 2002; Verpoorte and De Rooij 2003; Mutlu et al. 2004]. Continuous-flow systems are adequate for many well-defined and simple biochemical applications, and for certain tasks such as chemical separation [Wang et al. 2005], but they are less suitable for tasks requiring a high degree of flexibility or complicated fluid manipulations [Thorsen et al. 2002; Verpoorte and De Rooij 2003]. These closed-channel systems are inherently difficult to integrate and scale because the parameters that govern flow field vary along the flow path

making the fluid flow at any one location dependent on the properties of the entire system. Moreover, unavoidable shear flow and diffusion in microchannels makes it difficult to eliminate inter-sample contamination and dead volumes. Permanently etched microstructures also lead to limited reconfigurability and poor fault tolerance capability. Therefore, the fabrication of complex yet reliable continuous-flow biochips remains a major technical challenge.

**2.1.2 Digital Microfluidics.** Alternatives to the above closed-channel continuous-flow systems include novel open structures, where the liquid is divided into discrete, independently controllable droplets, and these droplets can be manipulated to move on a substrate [Pollack et al. 2000; Cho et al. 2002; Jones et al. 2001]. By using discrete unit-volume droplets, a microfluidic function can be reduced to a set of repeated basic operations, that is, moving one unit of fluid over one unit of instance. This “digitization” method facilitates the use of a hierarchical and cell-based approach for microfluidic biochip design. In this scenario, we envisage that a large-scale integrated digital microfluidic biochip can be constructed out of repeated instances of well-characterized unit cells in the same way that complex VLSI circuits may be built upon well-characterized transistors. Moreover, the constituent microfluidic unit cells, referred to as microfluidic modules, can be reorganized at different levels of hierarchy to support biochemical applications of various scales. Defect/fault tolerance is also easily incorporated in the design due to the inherent dynamic reconfigurability. Therefore, in contrast to continuous fluid flow, digital microfluidics offers a flexible and scalable system architecture as well as high defect-tolerance capability.

A number of methods for manipulating microfluidic droplets have been proposed in the literature [Gallardo et al. 1999; Ichimura et al. 2000; Sammarco and Burns 1999; Wixforth and Scriba 2002; Washizu 1998; Jones et al. 2001]. Of these, electrical methods to actuate droplets appear to be the most promising [Pollack et al. 2000; Cho et al. 2002; Washizu 1998; Jones et al. 2001; Vykoukal et al. 2001]. Dielectrophoresis (DEP) and Electrowetting-on-dielectric (EWOD) are the two most common electrical methods. DEP relies on the application of high-frequency AC voltages [Jones et al. 2001; Vykoukal et al. 2001] to modulate the dipole distribution in media, which gives rise an electrohydrodynamic force. EWOD uses DC (or low-frequency AC) voltages to modulate the interfacial tension at the tri-phase contact line where two immiscible fluids meet the dielectric layer coated over the solid electrode.

A unit cell of an EWOD-based digital microfluidic biochip consists of two parallel glass plates, as shown in Figure 1(a). The bottom plate contains a patterned array of individually controllable electrodes, and the top plate is coated with a continuous ground electrode. A dielectric, for example, parylene C, coated with a hydrophobic film of Teflon AF, is added to the plates to decrease the wettability of the surface and to add capacitance between fluids and the control electrode [Pollack 2001]. The droplet containing biochemical samples and the filler medium, such as the silicone oil, are sandwiched between the plates; the droplets travel inside the filler medium. In order to move a droplet, a control voltage is applied to an electrode adjacent to the droplet, and at the same time, the electrode just under the droplet is deactivated. The EWOD effect causes the

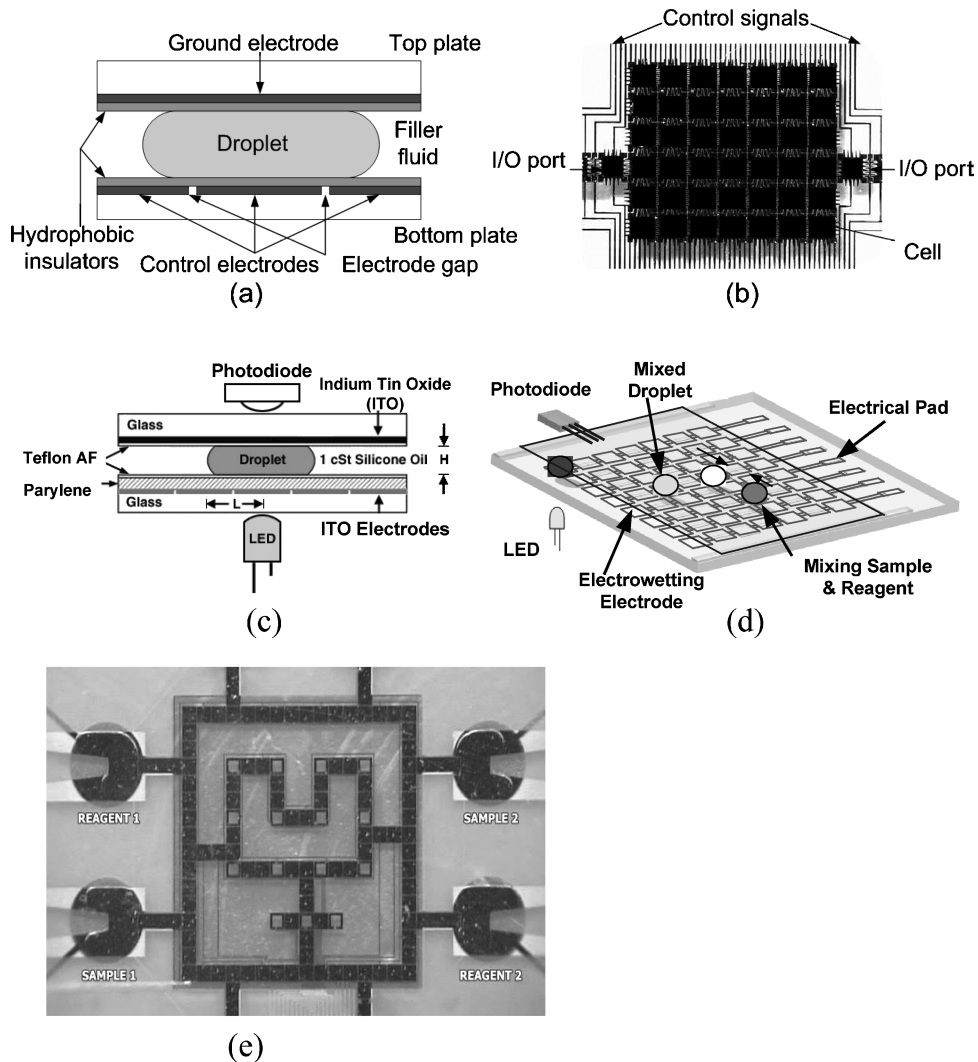


Fig. 1. EWOD-driven digital microfluidic biochip used for colorimetric assays. (a) and (b) illustrates the on-chip droplet manipulation. (a) shows the basic unit cell and (b) shows the two-dimensional array architecture. (c) and (d) illustrates the on-chip integration of optical detection. (c) shows the basic unit cell and (d) shows the two-dimensional array architecture. (e) shows the micrograph of the fabricated microfluidic array used for multiplexed bioassays.

transportation of the droplet. By varying the electrical potential along a linear array of electrodes, electrowetting can be used to move nanoliter volume liquid droplets along this line of electrodes [Pollack 2001]. The velocity of the droplet can be controlled by adjusting the control voltage (0~90 V), and droplets can be moved at speeds of over 20 cm/s [Pollack et al. 2002]. Droplets can also be transported, in user-defined patterns and under clocked-voltage control, over a two-dimensional array of electrodes. Videos on various microfluidic operations are available on the web at [www.ee.duke.edu/research/microfluidics](http://www.ee.duke.edu/research/microfluidics).

The in-vitro measurement of glucose and other metabolites, such as lactate, glutamate and pyruvate, is of great importance in clinical diagnosis of metabolic disorders. A colorimetric enzyme-kinetic glucose assay has been recently demonstrated in lab experiments on a digital microfluidic biochip [Srinivasan et al. 2003a, 2003b, 2004]. This biochip integrates an optical detection system consisting of an LED and a photodiode; see Figures 1(c) and 1(d) [Srinivasan et al. 2003a, 2003b, 2004]. In addition, glucose, lactate, glutamate and pyruvate assays can be combined to form a set of multiplexed bioassays that are performed concurrently on a microfluidic platform. Figure 1(e) illustrates a fabricated microfluidic system used for multiplexed bioassays [Srinivasan et al. 2004]. The concurrent execution of glucose and lactate assays has been demonstrated on this platform. Assays involving whole blood cells have not yet been successfully demonstrated by electrowetting [Srinivasan 2005]. Despite these limitations, advances in design automation tools will allow the design and fabrication of generic microfluidic platforms to which a set of assays can be mapped for optimized throughput, resource utilization, and fault tolerance.

There are natural similarities between digital microfluidic arrays and reconfigurable computing systems based on field-programmable gate arrays (FPGAs). However, the “programmability” of FPGAs is limited by the well-defined roles of interconnect and logic blocks. Interconnect cannot be used for storing information and logic blocks cannot be used for routing. In contrast, the microfluidics architecture that we are developing offers significantly more programmability. The unit cells can be used not only for storage and functional operations, but also for transporting fluid droplets.

Reconfiguration techniques for microfluidic arrays are also fundamentally different from the redundancy-based methods (spare rows/columns) used for memories, processor arrays, and FPGAs. Due to the absence of programmable interconnects such as switches between microfluidic cells, a droplet is only able to move directly to the adjacent cells. This property of fluidic locality implies that the functionality of a faulty unit cell can only be assumed by its physically neighboring cells in the array. Fluidic locality limits the reconfiguration capabilities of the spare rows/columns if they are not adjacent to the faulty cell.

## 2.2 CAD Trends and Challenges

While design tools for micro-electro-mechanical systems (MEMS) have reached a certain level of maturity, CAD tools for microfluidic biochips are still in their infancy. Some design automation techniques have been proposed for DNA probe arrays [Kahng et al. 2003]; however, microfluidics-based biochips are more versatile and complex than DNA arrays.

To date, most CAD research for microfluidic biochips has been limited to device-level physical modeling of components [Chatterjee and Alurn 2003; Shapiro et al. 2003; Zeng and Korsmeyer 2004], where device simulations based on computational fluid dynamics (CFD) play a central role. Besides home-grown prototype software, commercially available microfluidic CAD tools are broadly adapted in device design because they present the path of least resistance to high-quality complex device simulation solutions. Example commercial CAD

tools are CoventorWare (<http://www.coventor.com/microfluidics>), CFD-ACE+ (<http://www.cfdrc.com>), and FemLab (<http://www.comsol.com/>). Collectively, their simulation capability covers both generations of microfluidic biochips and actuation mechanisms derived from multiple domains of physics. Some simulation examples can be found in Section 4 of this article as well as Zeng and Korsmeyer [2004].

While state-of-art device simulation capability is quite powerful owing to the many years of development of CFD, the development of compact model library and system level synthesis and simulation still needs attention. Even though research on reduced-order modeling and system synthesis for microfluidic systems is an active research area (e.g., Chatterjee and Alurn [2005]; Wang et al. [2005] and Turowski et al. [2001]), commercial CAD tools for system-level microfluidic simulation are far from mature compared to the device simulation counterparts. To our knowledge, the Fluidic Architect offered by Coventor is the only system simulation platform that is commercially available [ConventorWare].

Short of a compact-model-rich library to support a system-level simulation at the start of a design, current design methodologies for microfluidics-based biochips are typically full-custom and bottom-up in nature. Detailed device simulations are used extensively to design and optimize the component and device, and to help to create custom compact models for this device. Once the devices are optimized using detailed physical simulation, they can be used to assemble a complete microfluidics-based biochip. Only at this stage, the system-level simulations and optimizations can be carried out. Since the system behavior can only be verified at such a late stage, costly and time-consuming redesign effort is required if the system does not satisfy design constraints.

Although these full-custom and bottom-up methodologies have been employed successfully in the past, they are clearly inadequate for the design of complex microfluidics-based biochips. For this, the top-down design methodology and design tools are called for.

### 3. AUTOMATED TOP-DOWN DESIGN

#### 3.1 Top-Down Design Methodology

The framework of the top-down design methodology for microfluidics-based biochips is illustrated in Figure 2.

The design starts at the bioassay protocols provided by the biochip users (e.g., biochemists). A sequencing graph model can be generated to describe this assay protocol, where the vertex set is in one-to-one correspondence with the set of assay operations and the edge set represents dependencies between assay operations. This model can be used to perform behavioral-level simulation to verify the assay functionality at the high level [Zhang et al. 2002].

Next, a synthesis tool is used to generate detailed implementations from the sequencing graph model. A microfluidic module library is also provided as an input of the synthesis procedure. This module library, analogous to a standard cell library used in cell-based VLSI design, includes different microfluidic functional modules, such as mixers and storage units. Compact models are used to

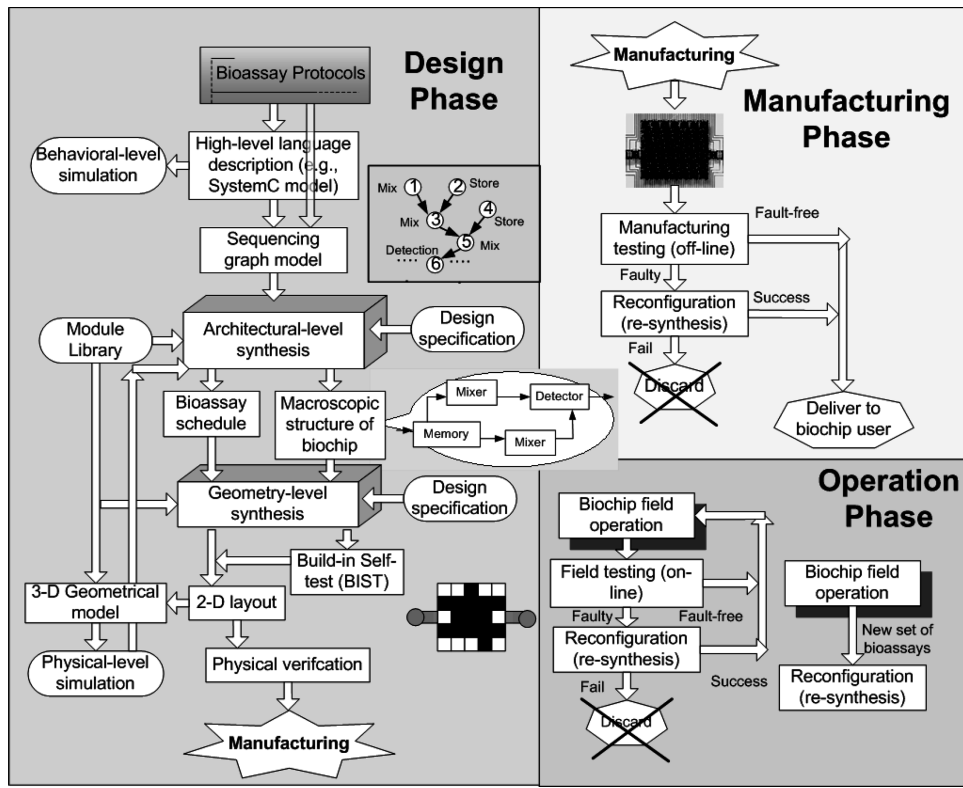


Fig. 2. Overview of top-down design methodology.

describe the behavior of individual modules, and are characterized by the module's function (mixing, storing, detection, etc.) and parameters such as width, length and operation duration through device simulations or laboratory experiments. In addition, some design specifications are also given *a priori*, for example, an upper limit on the completion time, an upper limit on the size of chip footprint, and the set of non-reconfigurable resources such as on-chip reservoirs/dispensing ports and integrated optical detectors.

The above synthesis flow includes both architectural-level synthesis (e.g., scheduling and resource binding) [Su and Chakrabarty 2004] and geometry-level synthesis (e.g., module placement and routing) [Su and Chakrabarty 2005a]. The output of the synthesis process includes a mapping of assay operation to on-chip resources, a schedule for the assay operations, and a 2-D biochip physical design (e.g., the placement of the modules). The synthesis procedure attempts to find a desirable design point that satisfies the input specifications and also optimizes some figures of merit, such as performance and area.

In addition, two important design issues must be incorporated into the system synthesis procedure. First, design for testability must be considered. A test plan and a set of test hardware (e.g., test droplet sources/sinks and capacitive detection circuits) associated with the synthesized assay operation and biochip physical design must be determined and integrated into the design [Su et al.

2004a, 2004b]. Second, design for fault-tolerance and manufacturability considerations are important. Microfluidic biochips are fabricated using standard microfabrication techniques. Due to the underlying mixed technology and multiple energy domains, they exhibit unique failure mechanisms and defects. A manufactured microfluidic array may contain several defective components, for instance, caused by dielectric breakdown and electrode degradation. Test and reconfiguration techniques can be used to bypass faulty components to tolerate not only manufacturing defects but also operational faults. Bioassay operations bound to these faulty resources in the original design can be remapped to other fault-free resources such that the defective biochip can be used, and thereby lead to higher yield and lower cost. The system-level synthesis flow must enable alterations in the resource binding operation and scheduling accounting for the strict resource constraints in an already-fabricated biochip.

After synthesis, the 2-D physical design of the biochip (i.e., module placement and routing) can be coupled with detailed physical information from the module library (associated with some fabrication technology) to obtain a 3-D geometrical model. This model can be used to perform physical-level simulation and design verification at a low level. After physical verification, the biochip design can be sent for manufacturing.

### 3.2 CAD for Top-Down Design

A complete design automation environment that enables the top-down design methodology is composed of multiple layers of functional modules [Senturia 1998], including:

- (1) *Technology CAD (TCAD)*. This usually includes a two-dimensional layout creation tool and a process modeling tool. Its major tasks are (i) to create three-dimensional device geometry from layout and process definition (process to geometry) and (ii) to identify optimal processes given desired device geometry (geometry to process).
- (2) *Device Simulation Tools*. Occasionally, this is also referred to as “FEM analysis modules”. Three-dimensional device geometry is discretized into a set of small cells or elements (“meshes”), based on which, a set of partial differential equations (PDE) that describe the corresponding domain physics (e.g., hydrodynamics, mechanics or electrostatics) or coupled multidomains of physics (e.g., electro-kinetics, fluid structure interaction) will be solved numerically. Device simulation usually offers high-fidelity predictions of the device behavior under the given operating condition.
- (3) *Library of Compact Models; Compact Model Construction Mechanism*. A compact model is also referred to as reduced-order model. It consists of *primitive models*, *macromodels* and *behavioral models*. It describes the device behavior via a small set of ordinary differential equations and/or algebraic equations (DAE). Compared to PDE-based device simulation, a DAE-based compact model offers higher level of abstraction, much faster simulation, and less geometrical flexibility. Three methods, namely

*System Design Specification*

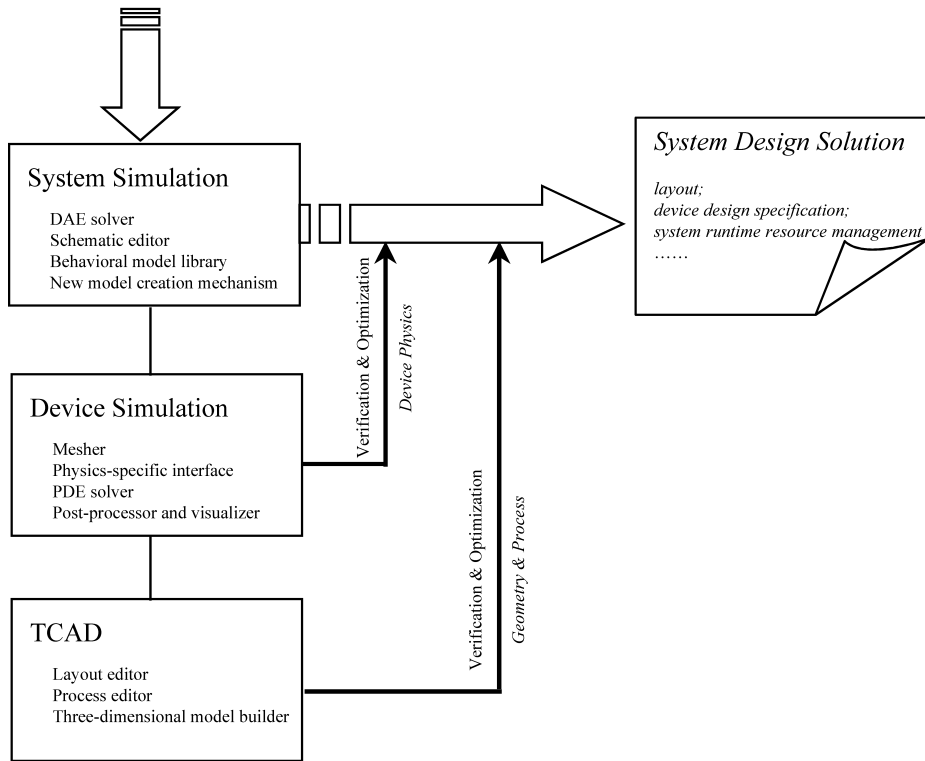


Fig. 3. An integrated top-down design automation environment for microfluidic biochips.

analytical methods, automated macromodel extraction, and Krylov-subspace-based automated model-order reduction, can be used to create compact models.

- (4) *System-Level Simulation Tools.* This enables assembly of compact models to form a system schematic. A system schematic illustrates a system representation graphically, and describes the system's dynamic behavior via DAEs (from compact models) and algebraic equations (from the connections between compact models). System simulation solves this set of differential algebraic equations and offers predictions of system behavior and performance. Furthermore, it provides guidelines for system optimization.

Figure 3 illustrates the CAD structure and its support for the top-down design paradigm.

The next three sections are focused on the development of the top-down design automation tools. Section 4 is focused on device simulation. It starts with an overview of microfluidic physics, followed by an overview of commonly adopted numerical methods, and concludes with a list of example applications. Section 5 emphasizes compact models and system-level simulation. It starts with an overview of system-level simulation, and is followed by an overview of

compact model creation mechanisms. The section concludes with examples of current practices.

Even though most of the examples are drawn from our own work, we will offer references to related studies to provide the readers with a broad perspective. The examples shown in Sections 4 and 5 are generated by the design automation CAD package CoventorWare® (Coventor, Inc., Cambridge, Massachusetts, USA), specifically Bubble-DropSim™ module for device simulation, and Fluidic Architect™ module for system simulation. FLOW-3D® (Flow Science Inc., Santa Fe, New Mexico, USA) is embedded in Bubble-DropSim as its multiphase-flow hydrodynamics solution engine. Fluidic Architect includes a microfluidic compact model library developed by Coventor, and the mixed-signal system simulation tool Saber® (Synopsys, Inc., Mountain View, California, USA).

## 4. DEVICE SIMULATION

### 4.1 Overview of Microfluidic Theory

The essence of biochip technology is to utilize streams of fluids (e.g., in channel-based biochips) or droplets (e.g., in digital microfluidics) as carriers of biochemical samples to carry out predetermined sample manipulation procedures. Microfluidics, according to fluid mechanics researchers [Stone et al. 2004], is “devices and methods for controlling and manipulating fluid flows with length scales less than a millimeter”. Owing to the fact that the fundamental operating principle of biochips is microfluidics and the dominating application of microfluidics is biochip design and development, microfluidics is regarded as a moniker inter-changeable with *biochip*, *lab-on-a-chip* or *micro-total-analysis systems* [Verpoorte and De Rooij 2003]. Next, we discuss several topics in microfluidic theory to highlight the two characteristics of microfluidics, that is, (i) microscopic length scale; and (ii) multiphysics hydrodynamics.

**4.1.1 Fluid Dynamics.** This is the essential component of microfluidics. The fundamental governing equations are Navier-Stokes equations that are derived from the conservation of mass, momentum and energy [Batchelor 2000]. When an interface that separates a gas and a liquid, or different types of liquids is present, an additional hydrodynamic constraint is applied in the form of an interfacial stress [Leal 1992]. In essence, the tangential component of the interfacial stress is continuous across the interface, and the discontinuity of its normal component is balanced by the pressure difference across the interface. The presence of the interface and the additional interfacial condition is also referred to as the surface tension effect.

**4.1.2 Issues Arising from Miniaturization.** The aspect ratio of fluidic components in a biochip is usually very large. In the cases of channel-based biochips, the length of the channel is much larger than the width and the depth. In the cases of digital microfluidics, the depth is much smaller than the dimensions of the reaction surface. In other words, large surface-to-volume ratio is a common characteristic for biochip architectures. The Navier–Stokes momentum equation states the balance among the momentum component (in the form of

volumetric integral), the viscous component (in the form of integration over the surface boundaries of the fluidic components), and the external driving force (pressure gradient, electric force, etc.). A large surface-to-volume ratio of the structure results in the dominance of the viscous effect over the momentum effect. Microfluidic flow is usually a low Reynolds number flow.

The presence of an interface creates a pressure difference across the interface, the magnitude of which is given by the surface tension coefficient multiplied by the curvature of the interface. The curvature of a macroscopic interface is usually small therefore such surface-tension-driven pressure difference is usually negligible compared to other sources. On the contrary, a microscopic interface possesses a very large curvature resulting a large surface-tension-driven pressure difference. To better illustrate this, considering an interface residing in a channel. When the cross-section dimension of the channel is in the order of a centimeter, the surface-tension-driven pressure difference across the interface is in the order of 10 Pa. When the channel shrinks such that the cross-section is in the order of 10 microns, the surface-tension-driven pressure difference across the interface now is in the order of 10 KPa. The dominance of the surface tension effect is one of the key consequences of miniaturization.

For most macroscopic flows, it has been (appropriately) assumed that there is no relative motion between the fluid particle and the solid at the fluid-solid boundary. This is the no-slip boundary condition. However microfluidic experiments show this no-slip boundary condition does not hold for a microscopic flow [Choi et al. 2003]. Rather, in microfluidics, a fluid particle at the fluid-solid boundary moves with a slip velocity relative to the solid surface, and the magnitude of this slip velocity is linearly proportional to the shear strain rate at the fluid-solid boundary [Navier 1823; Maxwell 1879; Lauga and Stone 2003].

**4.1.3 Electrokinetics.** The first successful demonstration of biochips was the separation of chemical samples based on capillary electrophoresis [Manz et al. 1992; Jacobson et al. 1994; Harrison et al. 1993]. Electrolyte, liquid containing charged chemical samples, is placed in a capillary where an electrical voltage difference is applied between both ends. With the presence of an electrical field, the charged species move relative to the liquid with different speed according to their different electromobilities. This is called *electrophoresis* and is one of the fundamental principles of on-chip separation analysis. In addition, the chemical state of the capillary wall is altered by the electrolyte such that the capillary wall acquires charges and releases the counter-ions to the liquid. The balance between the electrostatic interactions and the thermal agitation results a charged layer adjacent to the capillary wall. This layer is called the *Debye layer*. Outside the Debye layer, the electrolyte is electrically neutral therefore there exists no net electrical force. However, inside the Debye layer, a net charge density is present which together with the applied electrical field tangential to the capillary wall generates a net electrical force. This electrical force inside the Debye layer generates a bulk flow of the liquid and moves the electrolyte from one end of the capillary to the other. This is called *electroosmosis*. Electroosmosis not only provides a pumping mechanism, but the plug flow velocity profile of the resulting electroosmotic flow (EOF) contributes much less

distortion to the band shape of the species than the parabolic flow profile of a pressure-driven flow.

Both electrophoresis and electroosmosis are *electrokinetic* phenomena. Electrokinetics is hydrodynamics of electrolyte fluids in the presence of an electrical field.

The electric field may be described by electro-quasi-statics (EQS), and the governing equation is a truncated version of Maxwell's equations under the electroquasistatic assumption [Haus and Melcher 1989]. Typically, biochips operate at a small length scale (order of micrometer) and low frequency (order of MHz), therefore the electroquasistatic assumption is appropriate. The hydrodynamics is governed by Navier-Stokes equation augmented with one additional forcing term  $\mathbf{f}^{EK}$ , a force density of electrical origin, to the momentum equation.  $\mathbf{f}^{EK}$  is given by the net charge density  $\rho_e$  multiplied by the local electrical field intensity  $\mathbf{E}$ . Considering one type of ion present in the electrolyte, its contribution to the charge density is given by its concentration multiplied by the ion's (signed) valance and the charge on a proton.  $\rho_e$  is calculated by the summation of the contributions of all species. The transport equation governing the concentration of the species has three components: advection with fluid flow, diffusion relative to the fluid flow, and electrophoresis.

The governing equation of electrokinetics has three components: EQS, hydrodynamics, and species transport. These three components are coupled to each other: the presence and migration of charge affect electrical field; the product of charge and electrical field affects the hydrodynamics; the migration of the charge is determined by the transport of chemical species, which is function of both fluid velocity and electrical field [Saville 1977].

The thickness of the Debye layer is usually much smaller than the characteristic length of the biochip, therefore the electroosmotic effect can be approximated by a boundary condition applied at the solid-electrolyte interface. The liquid particle at the solid surface is assigned to a tangential velocity ("effective slip velocity") given by the local electrical field multiplied by a coefficient, the electroosmotic mobility, which is determined by the balance of  $\mathbf{f}^{EK}$ , and viscous shear inside the Debye layer [Karniadakis and Beskok 2001; Probstein 1994].

**4.1.4 Electrohydrodynamics.** The two leading architectures of digital microfluidics, that based on dielectrophoresis(DEP) [Jones et al. 2001; Schwartz et al. 2004], and that based on electrowetting-on-dielectric (EWOD) [Pollack et al. 2000; Cho et al. 2002; Prins et al. 2001], are applications of electrohydrodynamics to biochips [Zeng and Korsmeyer 2004; Jones 2002]. Digital microfluidics uses discrete fluid particles, droplets, as operands. Minute amounts of chemical sample are drawn from individual sample reservoirs in the form of metered droplets (picoliter to nanoliter). These droplets are then delivered to a reaction chamber where multiple droplets may reside simultaneously. When droplets containing different chemical samples arrive at the same location, the droplets merge into one droplet and a chemical reaction can occur. Chemical reactions can be detected, categorized, and reported. Hierarchical reactions can be achieved by merging droplets of intermediate reactions. A larger droplet may be split into smaller ones for parallel manipulation or detection. An individually

addressable electrode array generates a pre-programmed electrical field, which exerts electrohydrodynamic forces on fluids to accomplish the aforementioned operations.

Compared to electrokinetics where the fluid contains electrolytes and the fluid flow is driven by Coulomb's Force, electrohydrodynamics can be better understood from an energy perspective. The presence of the electrical field leads to the storage of electrostatic energy in media. An EWOD chip places two immiscible fluids (e.g., water and air) on top of a solid surface. If the two fluids possess different electrical properties, the electrical fields (hence, the density of the stored electrostatic energy) in solid underneath these two fluids are different. The energy disparity right underneath the tri-phase contact line generates hydrodynamic force, which acts on the tri-phase contact line and moves the contact line advancing towards the fluid with less permittivity [Adamson 1990; Verheijen and Prins 1999]. DEP originates from the redistribution of the dipole moment in the medium by an external electrical field. By re-aligning the direction of the dipole moment and the relative movement of the paired charges, the electrostatic energy is injected into the medium. A disparity of the electrostatic energy density gives rise to a hydrodynamic force [Pohl 1978].

Similar to electrokinetics, electrohydrodynamics can also be explained using coupled physics between electrostatics (EQS) and hydrodynamics. The governing equations of EQS and hydrodynamics are coupled through an electrohydrodynamic force density  $\mathbf{f}^{\text{EHD}}$ , which equals the gradient of the stored electrostatic energy.  $\mathbf{f}^{\text{EHD}}$  is the additional forcing term for the momentum equation that governs the hydrodynamics.  $\mathbf{f}^{\text{EHD}}$  drives the fluid flow, and fluid flow modifies the electrical property distribution in space hence the electrical field, which in turn alters  $\mathbf{f}^{\text{EHD}}$  [Hans and Melcher 1989; Melcher 1981; Landau and Lifshitz 1960; Melcher and Taylor 1969].

**4.1.5 Thermocapillarity.** The temperature dependency of surface tension causes fluid to move in a liquid/gas/solid system. This thermocapillary effect has also been adopted as an operating principle for digital microfluidics. An on-chip temperature gradient can be established and modulated via an array of embedded micro heaters (thermal conduction) or an array of laser sources (radiative heating). A droplet on chip moves towards the colder region [Darhuber et al. 2003; Valentino et al. 2005; Chen et al. 2004; Nguyen and Huang 2005; Tseng et al. 2004]. Compared to EWOD, thermocapillarity modulates the interfacial energy density on the fluid–fluid interface, whereas EWOD modulates the interfacial energy density on the fluid–solid interface.

The governing equations for thermocapillarity include multiphase hydrodynamics (where surface tension force along with other hydrodynamic forces dictates the flow), thermal analysis (where the heat conducts among all three phases and simultaneously the heat convection occurs with the flow), and the constitutive equation that describes the temperature dependency of the surface tension coefficient.

**4.1.6 Fluid-Structure Interaction.** A pumping mechanism is required by almost every biochip design [Laser and Santiago 2004]. It may be loosely

categorized in two families: the *dynamic pumping*, examples being centrifugal pumps [Zoval and Madou 2004], pumps based on aforementioned electroosmosis [Zeng et al. 2001], electrohydrodynamics [Jones 1973], and magnetohydrodynamics [Homsy et al. 2005]; the *displacement pumping*, where a movable structure (diaphragm) is integrated on-chip to push fluids, and the motion of the structure is controlled piezoelectrically (e.g., one of the earliest micropumps by Smits [1990]), electrostatically [Xie et al. 2004], or others (e.g., via thermal bi-morph).

The governing principle of displacement pumping is *fluid-structure interaction*. The structural dynamics has three components: the driving mechanism, e.g., piezoelectrics, electrostatics; the elasticity of the diaphragm; and the coupling with the hydrodynamics. On the hydrodynamics side, the no-slip condition at the fluid-solid interface forces the fluid to move with the diaphragm. On the structural dynamics side, the hydrodynamic forces (the hydrodynamic pressure and the viscous shear) exerted on the diaphragm determine the transient displacement of the diaphragm [Pan et al. 2002].

## 4.2 Overview of Numerical Methods

Microfluidic theory is expressed mathematically in the form of a set of partial differential equations, and solved numerically via generalized computational fluid dynamics (CFD), which includes not only numerical methods for Navier–Stokes equations [Andorson 1995], but also for other domains of physics such as computational structural mechanics and computational electrostatics. Numerical methods have three essential components: (i) representation and discretization of materials (meshing); (ii) discretization of the governing equations; and (iii) solution post-processing and visualization.

**4.2.1 Discretization of Computational Domain.** TCAD creates three-dimensional geometrical entities according to the layout and process information. Each geometrical entity contains one type of material. A *computational domain* is an enclosed three-dimensional volume. Geometrical entities inside the computational domain are considered “important” to the device behavior, therefore they are analyzed in detail. The geometrical entities outside of the computational domain are either considered have negligible contribution to device behavior or their contribution can be adequately represented by constraints applied to the surface of the computational domain (i.e., boundary condition). The discretization of a computational domain (*meshing*) creates a finite-size set of *cells* to represent the geometrical property and material property of the computational domain. A cell may be an element in finite element (FEM) or finite volume (FVM), or a brick formed by neighboring finite difference (FDM) grids. Mathematically, a cell is described by its *nodes*, *edges*, *faces* and *shape functions*. The accuracy of the numerical solutions is determined by both the cell size and cell quality (e.g., aspect ratio). An excellent review for computational domain discretization techniques was published by Thompson [1984].

When device performance involves movement and/or deformation of a material, for instance, diaphragm deflection of a microfluidic pump or droplet translocation on a digital microfluidics, the surface of a geometrical entity, or the

boundary of a material, undergoes kinetic, geometrical or topological change. There are two leading algorithms for accurately tracing the transient evolution of surfaces, the *surface tracking method* and the *surface capturing method*, associated with discretization of the computational domain. The *surface tracking* method [Hirt et al. 1974; Tezduyar et al. 1992a, 1992b] requires the nodes to be positioned on the surface of a geometrical entity such that the surface of the geometrical entity can be described explicitly by a set of cell faces. If this geometrical entity changes its location, geometry or topology, the cells adjacent to the surface need to be adapted such that the cell faces track the changed surface and simultaneously maintain good quality. On the contrary, the *surface capturing* method [Hirt and Nichols 1981] partitions the computational domain into a set of cells fixed in space. The cell faces do not have to overlap with the surface of the geometrical entity, and do not change with the evolution of the geometrical entity surface. Instead, an additional “color” function is defined on the cells to describe the distribution of the geometrical entity. The movement of the geometrical entity is represented by the change of this color function with time. The movement of the surface is not explicitly tracked by cells, rather, is captured by the evolution of a color function.

**4.2.2 Discretization of the Governing Equations.** Governing equations are discretized based on cells. The physical quantities (both knowns and unknowns) are defined on cell nodes, cell centers, or both (e.g., staggered grids). The space-dependent differential or integral operations of the governing equations are transformed into set of, linear or nonlinear, algebraic operations using *Finite Difference (FDM)*, *Finite Element (FEM)*, *Finite Volume (FVM)* or *Boundary Element (BEM)* methods. Consequently, the governing equations are transformed into set of ordinary differential equations (ODE) solely depending on time. The discretization of ODEs using either *implicit* or *explicit* scheme eventually leads to the final product of the discretization of governing equations: an algebraic system of equations, which are in turn solved by either *direct* or *iterative* methods. Iterative methods are necessary when the problem is nonlinear. *Preconditioning* and *multigrid* are the two leading algorithms that can accelerate the convergence rates for iterative method [Hirsch 1988].

The *Finite Difference method* is the oldest and most advanced method applied to solve differential equations numerically. The first application of FDM is believed to have been developed by Euler in 1768. FDM is based on the properties of Taylor expansions. The algebraic expressions of derivatives are obtained directly from the Taylor expansions. FDM requires structured cells such that all the cell nodes are the intersections of numerical coordinate curves and all the edges are unit segments of the numerical coordinate curves. The *Finite Element method* originated from the structural analysis; it was first formally elaborated by Turner et al. [1956], and was named by Clough [1960]. FEM can work with unstructured cells; however, it requires that cells not to overlap with each other. The distribution of the quantities inside a cell is expressed as a weighted summation of nodal quantities with the shape function as the weight. The mathematical base of FEM is functional analysis. FEM requires translating the governing equations into an integral formulation using a *variational*

*principle or a weak formulation*, also called the *method of weighted residuals* (e.g., *Bubnow–Galerkin method*). The *Finite Volume method* became part of CFD in the early 1970s [McDonald 1971; MacCormack and Paullay 1972]. FVM requires expressing the governing equations in the form of the integral forms of the conservation laws, and such integral equations are then directly discretized on cells. FVM works with both structured cells and unstructured cells. FVM can be considered as a special case of FDM, where the governing equations are written as differential, conservative form and discretized based on arbitrary co-coordinates; FVM can also be considered as a special case of FEM where collocation methods (a variant of a weak formulation) are used. The mathematical basis for *Boundary Element method* is the Green's function theory [Bebbia 1978]. It can be applied only to *boundary value problems* where the governing equations can be transformed into integration over the boundaries of the computational domain. BEM can solve a subset of hydrodynamic problems, where the Reynolds number is either extremely large (potential flow) or equals to zero (Stokes flow). Many of microfluidic problems find the latter case, the Stokes flow assumption, appropriate. The numerical implementation of BEM is similar to FEM, even though FEM works with three-dimensional cells and BEM works with two-dimensional surface cells.

**4.2.3 Solution Post-Processing and Visualization.** The solutions of the device simulation can be used to investigate device physics, validate the existing behavioral model, and/or serve as the basis to construct new behavioral model. Therefore, the visualization tool should enable easy access to solutions via both rendering the field data on device and probing the data at a desired location/cell. It should be able to work with multiple fields simultaneously to better expose the potential connections among different fields. In addition, the post-processing should include a spatial and temporal integration tool-kit that allows the integration of the field of interest over a desired spatial domain (a set of cells, faces of a set of cells, or edges of a set of cells) or time. This is particularly useful when validating an existing behavioral model. Construction of a new behavioral model based on the device simulation solution will be reviewed in Section 5.

### 4.3 Device Simulation Examples

**4.3.1 Centrifugal-Driven Channel-Based Micro Total Analysis System.** Figure 4(a) illustrates a compact-disk-(CD)-like microfluidic device. When spinning the disk, the centrifugal force will pump the liquid from the center of the disk towards the edge of the disk. Microchannel based microfluidic components (reservoir, channel, valve, reaction chamber, waste collection) are placed on the disk along the radial direction outwards. Passive capillary valves are used to gate the liquid flow. A capillary valve is an abrupt opening where the contact angle can become very large such that the surface tension force acts against the liquid flow. The control of the fluid flow is achieved by modulating the spinning velocity thus the centrifugal force. The liquid flow stops at the capillary valve when the centrifugal force, along with liquid momentum, is not strong enough to overcome the surface tension force [Zoval and Madou 2004; Duffy et al. 1999].

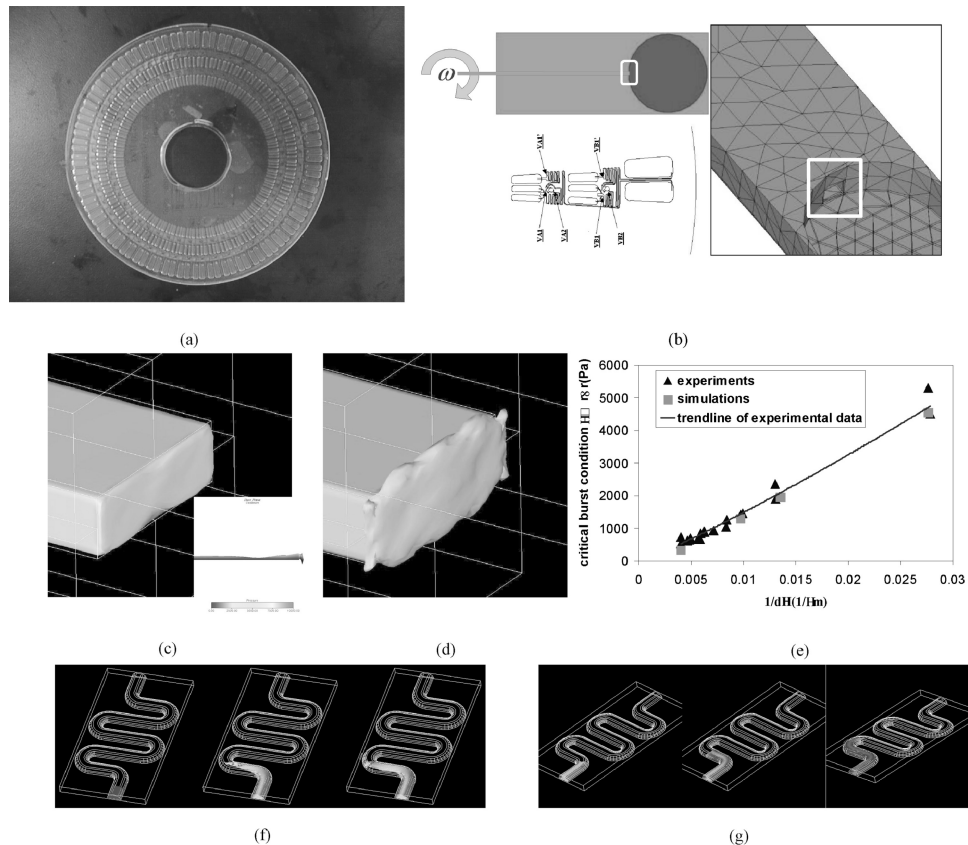


Fig. 4. Device simulation example: Centrifugal driven microfluidic compact disk. (a) shows the image of such device fabricated by Tecon Boston (formerly Gamera Bioscience). Courtesy Dr. Gregory J. Kellogg, [Zeng et al. 2000]. At lower left of (b) shows a slice of detailed micro-fluidic structure positioning on the rotating plate radically (courtesy Dr. Gregory J. Kellogg). The geometry of the capillary valve used in simulation is shown in (b) at right. (c) shows a steady-state meniscus shape when the capillary valve stops the liquid flow successfully. A slice plane is cut through the liquid body from the meniscus to the reservoir to record the pressure distribution. It shows the surface tension force suppresses the centrifugal pumping. (d) shows a meniscus shape where the capillary valve is broken when a higher spinning velocity is applied. (e) shows the maximum capillary barrier verses geometry of the capillary valve. Simulations are compared against experimental measurement (experimental data courtesy Dr. Gregory J. Kellogg). (f) and (g) show the centrifugal pumping of the liquid in a serpentine micro-channel. (f) shows the liquid jets at the turn and a bubble is entrapped. When the spinning velocity is reduced, (g) shows the interface propagates along with the channel wall and there is no bubble entrapped.

When designing a capillary valve, it is in the designers' interest to understand the critical burst condition, that is, the largest spinning velocity under which the surface tension force can prevent the liquid from flowing out of the valve ("burst"). Such a critical burst condition depends on the geometry of the abrupt opening and the distance between the valve and the disk center. It also depends on the material properties such as the surface tension and liquid kinetic viscosity. Device simulation is used to quantify the critical burst condition

[Zeng et al. 2000]. Figure 4(b) shows the geometry of an example capillary valve. Transient simulations are carried out and a slice plane cuts through the liquid body and reports liquid pressure to gauge if a steady-state is achieved for cases where the liquid flow is stopped by surface tension (Figure 4(c)). When the spinning velocity increases the liquid bursts out of the capillary valve, as shown in Figure 4(d). Figure 4(e) shows simulations sweeping through geometric parametric space and report the critical burst condition as function of the valve geometry characterized by the hydraulic diameter. Such simulation results describe the capillary valve behavior and can serve as foundation for behavior model creation. Figure 4(e) also shows good agreement between simulations and experiments.

The spinning velocity also controls the process of liquid filling in the microchannel. When the CD spins fast, the centrifugal pumping effect jets the liquid at the turn and a bubble is entrapped, as shown in Figure 4(f). When the spinning velocity is reduced, Figure 4(g) shows that the interface propagates along with the channel wall and the bubble entrapment is avoided.

**4.3.2 Liquid Flow in Microchannels.** Automated analysis of channel-based biochips is realized by the control of liquid flow through various microchannels. Device simulations are used to investigate the device behavior and to optimize the device design parameters [Erickson 2005]. Figure 5 illustrates several example device simulations for problems that are commonly encountered in the design of channel-based biochips.

T-channels are effective mixing components. One design problem is to find the optimal geometry (cross-section and length) for the T-channel such that desired flow rates are achieved with given pressure at the three ports. Figure 5(a) shows an example simulation of flow through a T-channel. Figure 5(b) shows a transient sequence of capillary filling of a T-channel, obtained from simulation. The T-channel is fabricated via isotropic etching having a D-shaped cross-section with rounded sidewall. Capillary filling process may entrap bubbles as shown in figure 4(f). The presence of bubbles introduces unwanted complication to flow control. Figure 5(c) is a simulation of a bubble removal procedure: a liquid flow flushes a bubble downstream. Figure 5(d) shows a transient simulation of sample mixing. Initially introduced into the channel as two adjacent plugs, two samples diffuse into each other while being carried by the liquid flow downstream.

**4.3.3 Electrified Droplets in Digital Microfluidics.** Digital microfluidics uses discrete fluid particles or droplets as carriers for biochemical agents to carry out various analytical procedures. Compared to the channel-based biochips, digital microfluidics is reconfigurable, scalable, and of general purpose. A complex on-chip analysis can be programmed by combining a small set of basic droplet manipulation instructions, and carried out in a manner similar to traditional bench-top protocols. The basic instruction set include droplet generation, or separating a liquid stream into discrete droplets; droplet translocation; droplet fusion, or merging multiple droplets into one; and droplet fission, or dividing one droplet into smaller ones.

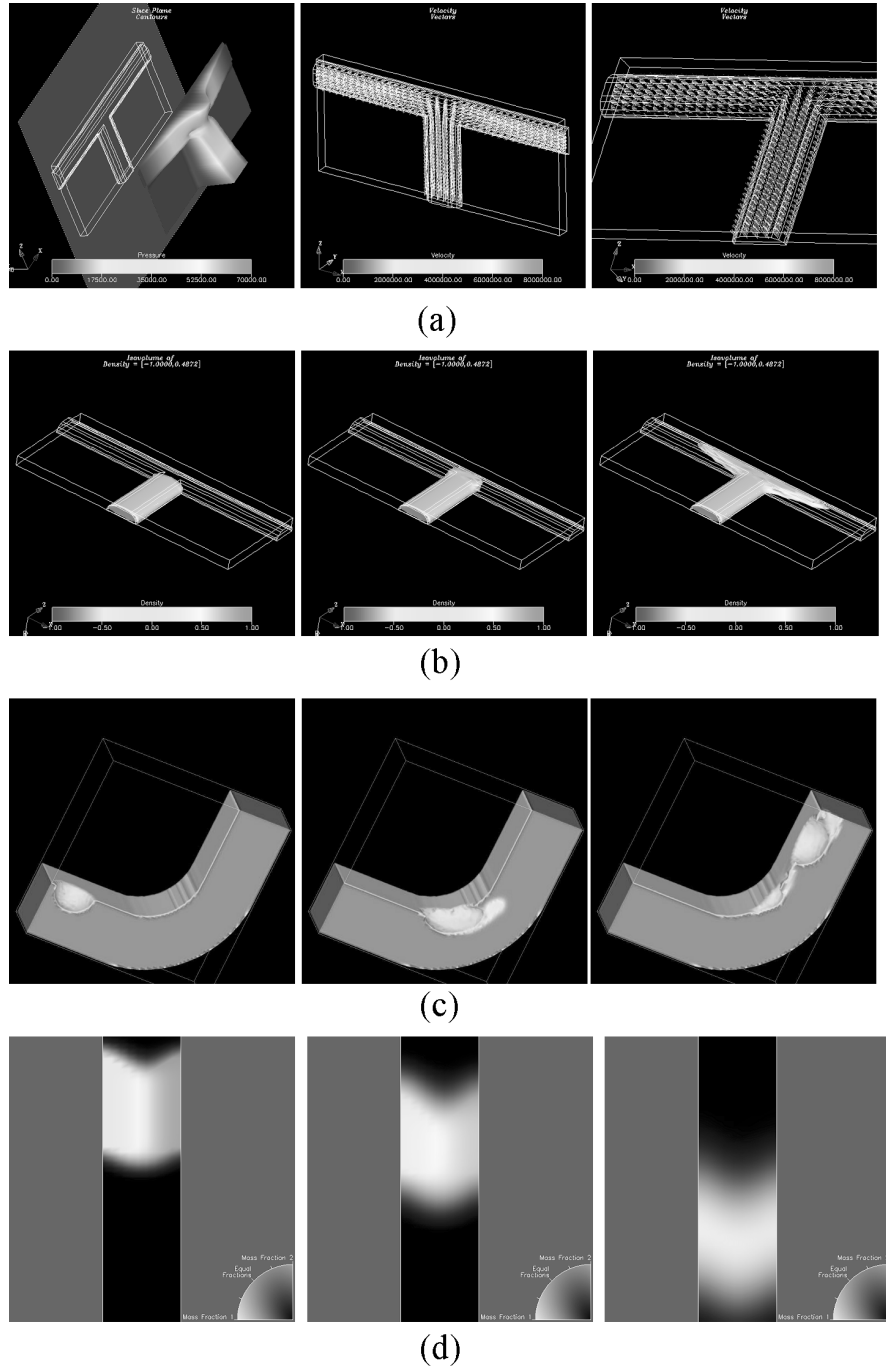


Fig. 5. Other device simulation examples on channel-based microfluidics. (a) Liquid flow in a T-channel, from left to right shows pressure field, velocity and a zoom-up view of the T-junction. (b) A transient sequence of liquid filling an initially vacant T-channel. (c) A transient sequence of a bubble being flushed downstream. (d) A transient sequence of mixing of two species.

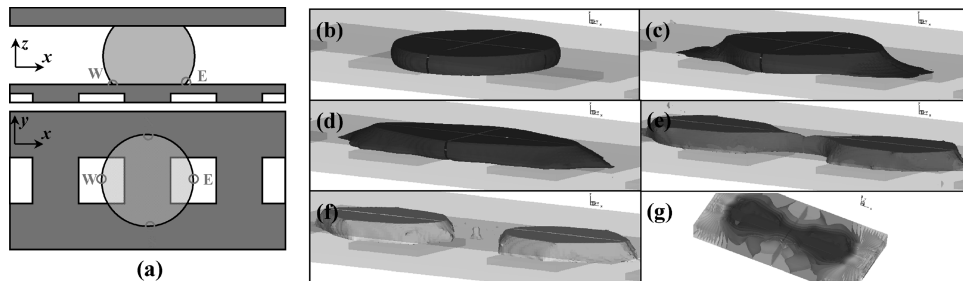


Fig. 6. Droplet fission on an EWOD-driven lab-on-a-chip. (a) illustrates the device configuration. All four electrodes embedded in the insulating material are ON electrodes. The square electrodes are 100  $\mu\text{m}$  wide and 100  $\mu\text{m}$  apart. The thickness of the insulating coating is 5  $\mu\text{m}$ . Initially (without the presence of the electric field) this droplet of 1  $\mu\text{L}$  is of a “pancake” shape maintaining a contact angle of 117°. (b)–(f) show the transient process of droplet fission (simulation), corresponding to times 0, 75, 150, 450 and 600  $\mu\text{sec}$ . Upon application of 70 V to all four electrodes, the reduction of the contact angle elongates the droplet in the  $x$  direction, shrinking the  $yz$ -plane cross-section at the center of the droplet, which eventually breaks the droplet into two parts. Satellite droplets can also be observed in (f). (g) shows the electric potential distribution (simulation) at time 450  $\mu\text{s}$  (corresponding to (e)). [Zeng et al. 2004].

Droplet binary fission, that is, one droplet being separated into two equal-volume smaller ones, is of particular interest to designers. The parallelization of the on-chip operation, including both multi-stage chemical analysis and detection, relies on a high-precision droplet binary fission to ensure the generated two droplets carry equal amount of chemical species. In addition, combination of multiple droplet fusion and droplet fission alternatively can enhance mixing of chemical species carried by the droplets [Paik et al. 2003].

Droplet binary fission is a phenomenon dictated by hydrodynamic interfacial instability. The precision of the fission process is very sensitive to the operating condition, device geometry, and material property. Device simulation can be used to analyze, for given device and material, the complex interdependency of the operation precision and the operating condition. Such understanding can further help to design better devices for a given type of material.

Figure 6 shows the simulation of a transient process of droplet binary fission on an EWOD-driven digital microfluidics chip [Zeng and Korsmeyer 2004]. Figure 6(a) illustrates the device geometry. The electrodes are aligned along the X direction, and a droplet initially is centered in between two neighboring electrodes. Upon application of a voltage to all the electrodes, a spatial disparity of EWOD force is created. The contact angle at the tri-phase contact point closer to the electrodes (the vicinity of points W and E) is smaller than that at the tri-phase contact point further from the electrodes (the vicinity of points N and S). Consequently, as shown in figure 6(b)–(f), the droplet is elongated in the  $x$  direction at both sides (along W–E plane), and simultaneously the Y–Z cross-section at the center of the droplet (on N–S plane) is reduced. Eventually the cross-section in the N–S plane reduces to a point and two droplets are created to conclude the fission process. Figure 6(g) presents the distribution of the electric potential in this EWOD-driven device.

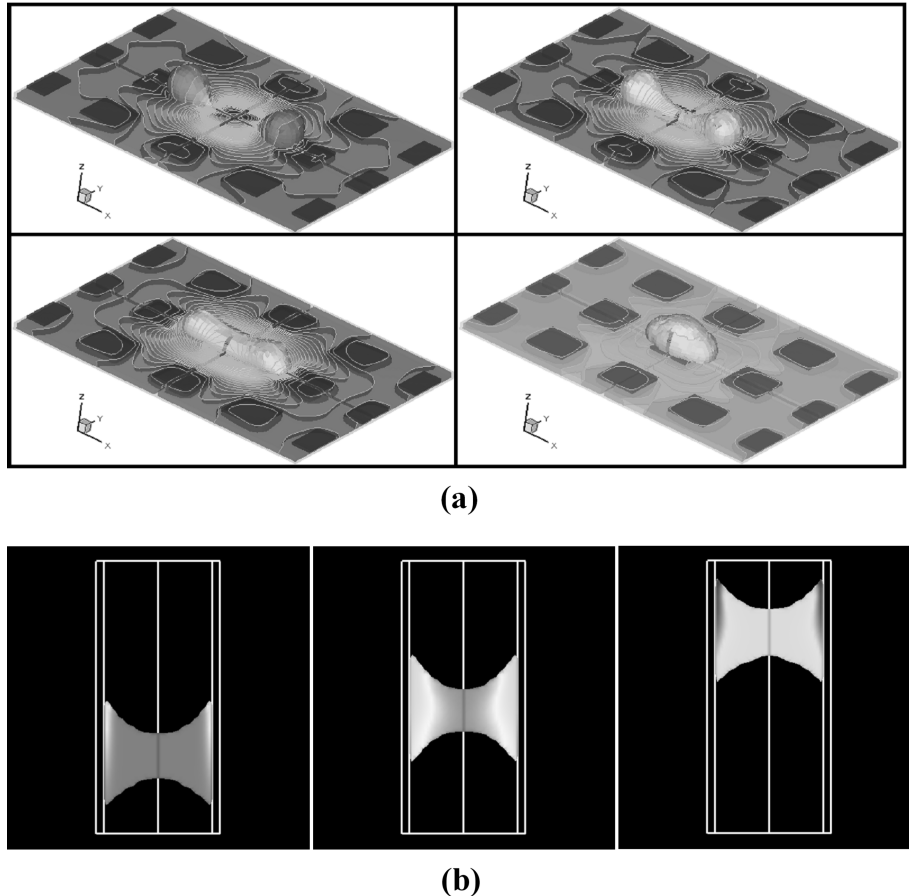


Fig. 7. Simulations of on-chip droplet manipulation. (a) Droplet fusion driven by DEP. (b) Droplet translocation driven by thermal capillarity.

Figure 7 shows simulation of on-chip droplet manipulation by DEP and thermocapillary effect.

## 5. SYSTEM SIMULATION

### 5.1 Overview of System Simulation and Reduced-Order Modeling

As discussed in the previous section, device simulation solves a set of partial differential equations that govern the device physics. Such numerical practice for a single device usually demands considerable computational resources (e.g., CPU, memory). A microfluidic system usually integrates a large number of devices. Consequently, the use of a device simulation approach to evaluate the performance of a microfluidic system demands a prohibitive amount of computational resources, which effectively makes device simulation unsuitable for system evaluation. The performance evaluation and optimization of a large-scale integrated microfluidic system relies on compact-model-based system

simulation. A system simulation environment has three essential components: (i) a *simulator* that can solve a large set of algebraic and/or ordinary differential equations; (ii) a *library* of compact models; and (iii) a mechanism for creating new compact models (*model creation*).

**5.1.1 Hardware Description Language and Simulator.** The dynamic properties of a microfluidic device and system are usually continuous in time, therefore can be best described by analog signals. In addition, digital events also occur in a microfluidic operation, for instance, the completion of droplet binary fission (Figure 6). Popular hardware description languages (HDL) for analog and mixed signal (AMS) design, simulation and verification, are MAST [Mantooth and Feigenbaum 1995] and Verilog-A [Fitzpatrick and Miller 1998]. Well-known simulators include SPICE from University of California, Berkeley, Simulink® from MathWorks, Saber® from Synopsys and Virtuoso® from Cadence.

**5.1.2 Compact Models.** A compact model of a device refers to a set of ordinary differential or algebraic equations (DAE) that describes the dynamic properties of this device as functions of time. A compact model is composed of a *symbol*, a graphical representation of this compact model where parameters can be specified to instantiate this compact model, and a *template*, where these set of DAEs are programmed in HDL in a parameterized fashion. A system *schematic* is a circuit-like graph representation of a system. Compact models are nodes of the graph representing devices that form this system. The edges among nodes represent the dynamic dependency, interfacing with the compact models via *cross variables* (e.g., hydrodynamic pressure) and *through variables* (e.g., flow rate).

There are three types of compact models, *primitive models*, *macromodels*, and *behavioral models*. Primitive models refer to the basic elements of a system, for instance, capacitors, inductors, resistors, transistors and their equivalences in other energy domains. A macromodel is a specific composition of primitive models enabling description of a new device.

A behavioral model is the most generic, and thus the most powerful form of a compact model. It describes the dynamic response of a device via a set of DAEs derived from the domain physics. Section 5.2 will describe a behavioral model example and illustrate the derivation procedure.

**5.1.3 Reduced-Order Modeling.** In real life, the dynamic behavior of a microfluidic device depends not only on time but also on the three spatial coordinates. The microfluidic dynamics is governed by partial differential equations with respect to four independent variables (time and space). A compact model of a microfluidic device solely depends on time. Reduced-order modeling refers to compact model generation procedures that lump the spatial dependency of a device behavior.

*Analytical methods* can be used to derive compact models. Starting from the physical insights into device behavior, a set of realistic assumptions can be made, which serve as the basis to simplify the PDE-based governing equations and reduce them into the form of DAE. This set of DAE-based governing

equations can be used directly for compact model creation. Section 5.2 shows an example of this approach.

Device simulation works directly with the PDE-based governing equations. The space-dependent differential or integral operations of the governing equations are transformed into a set of (linear or non-linear) algebraic operations using FDM, FEM, FVM or BEM. Consequently, the PDE-based governing equations are transformed into a set of ordinary differential equations (ODE) solely depending on time (Section 4.2). In principle, this set of ODEs can be used directly to create compact models. The size of this set of ODEs can be estimated by the number of the numerical cells multiplied by the number of unknowns, which can easily be tens of thousands to millions. The computational cost associated with a compact model created by this naïve approach makes such compact models infeasible in practice. On the other hand, this set of ODEs is created using a brute-force approach, where there may be wastage, for instance, too many cells for the desired accuracy, or possible simplification of dependencies among physical properties based on the desired accuracy. In other words, for many practical engineering problems and desired accuracy, one can expect to find a different set of ODEs with much smaller size that can effectively describe the device behavior. This new set of ODEs can be used directly for compact model creation. *Model order reduction* (MOR), the procedure that automatically generates this new set of ODEs of much smaller size from the original set of ODEs of extremely large size directly obtained from the device simulation discretization, is an active research field. Many MOR algorithms are derived using the Krylov subspace method. A review of MOR can be found in Rudnyi and Korvink [2002].

A microfluidic device may be described by an RLC circuit. Consider liquid flow in a long channel, a device usually encountered when constructing a channel-based microfluidic system. The momentum acceleration can be modeled as an inductor; the viscous shear from the channel wall can be modeled as resistor; and the compliance (the relationship between liquid volume and the applied pressure) can be modeled as a capacitor. Device simulation solutions can be used to identify the RLC values. For instance, a transient device simulation of liquid flow in the given channel under a constant pressure difference at both ends can provide the flow rate as function of time. The inductance can be calculated from the time derivative of the flow rate divided by the pressure difference. The procedure of automating the device simulation and RLC value extraction is called *automatic macro-model extraction* [Swart et al. 1998]. This is another way to create compact models.

## 5.2 Capillary Filling in Microfluidic Channels: An Example of Compact Model Creation and System Simulation

Capillary filling is commonly encountered in designing channel-based microfluidics system. Channel-based biochips utilize lengthy microchannels to deliver liquid solution. Before use, the channels are usually washed via flushing through water or solvent, and then dried by hot air. When used, the inlet of the biochip is connected with a buffer liquid reservoir. The surface tension

force will pull the liquid into the micro channels (provided the buffer liquid is “wetting” to the channel wall). Sometimes a syringe pump may be connected to the reservoir to apply a slight pressure to help drive the liquid into the micro channel.

Understanding the capillary filling process is important to biochip design. Different geometries of liquid flow pathways may result in different capillary filling behavior such as filling time, and the possibility of entrapment of air bubbles. Knowledge of the filling process can guide designers in arranging internal structures of the chip (such as chambers, binding pillars, splits, valves) to avoid potential filling problems and achieve higher filling speeds. While the design of an individual channel component can be carried out at the device simulation level as illustrated in Section 4.3, evaluating the filling process on the chip scale requires system level simulation and compact models that can describe filling behavior in a reduced-order fashion.

Consider a very long microchannel of rectangular cross-section partially filled with liquid. Initially (at time  $t = 0$ ), the length of the liquid inside the channel is  $L_0$ . The microchannel is shallow such that the width is much larger than the depth  $D$ . Therefore, it is reasonable to assume that the dependency of the microfluidics on the direction of width is negligible and this problem can be safely reduced to two dimensions in space.

The liquid is of density  $\rho$  and dynamic viscous coefficient  $\mu$ . The contact property between the liquid and channel wall is defined by surface tension coefficient  $\sigma$  and contact angle  $\theta$ . Surface tension force is one of the primary driving forces when the contact is hydrophilic, that is,  $\theta$  is smaller than  $90^\circ$ . A pressure difference of  $\Delta P$  (pressure overhead) is applied at the both ends of the channel to accelerate the filling process.  $\Delta P = 0$  defines a *passive capillary-filling* process.

Assuming that, at time  $t$ , the liquid length inside the channel reaches  $L$ , and the average filling velocity is  $u$ . The average filling velocity is defined by the liquid flow rate divided by the channel cross-section area. Therefore, the momentum of the liquid may be expressed as  $\rho D L u$ . The velocity is assumed to have a two-dimensional Poiseuille flow profile, therefore the viscous force can be expressed as  $-12\mu L u / D$ . The pressure force is  $\Delta P D$ , and the surface tension force is  $\sigma \cos(\theta)$ . The conservation of momentum may be expressed as the momentum change balanced by the summation of viscous force, pressure force and surface tension force:

$$\frac{d}{dt} (\rho D L u) = -\frac{12\mu L u}{D} + \Delta P D + \sigma \cos(\theta). \quad (1)$$

Noting that  $u = dL/dt$ , the above equation above can be rewritten as

$$\frac{d^2}{dt^2} L^2 + B \frac{d}{dt} L^2 = A, \quad (2)$$

where

$$A = \frac{4\sigma \cos(\theta) + 2\Delta P D}{\rho D}; \quad B = \frac{12\mu}{\rho D^2}. \quad (3)$$

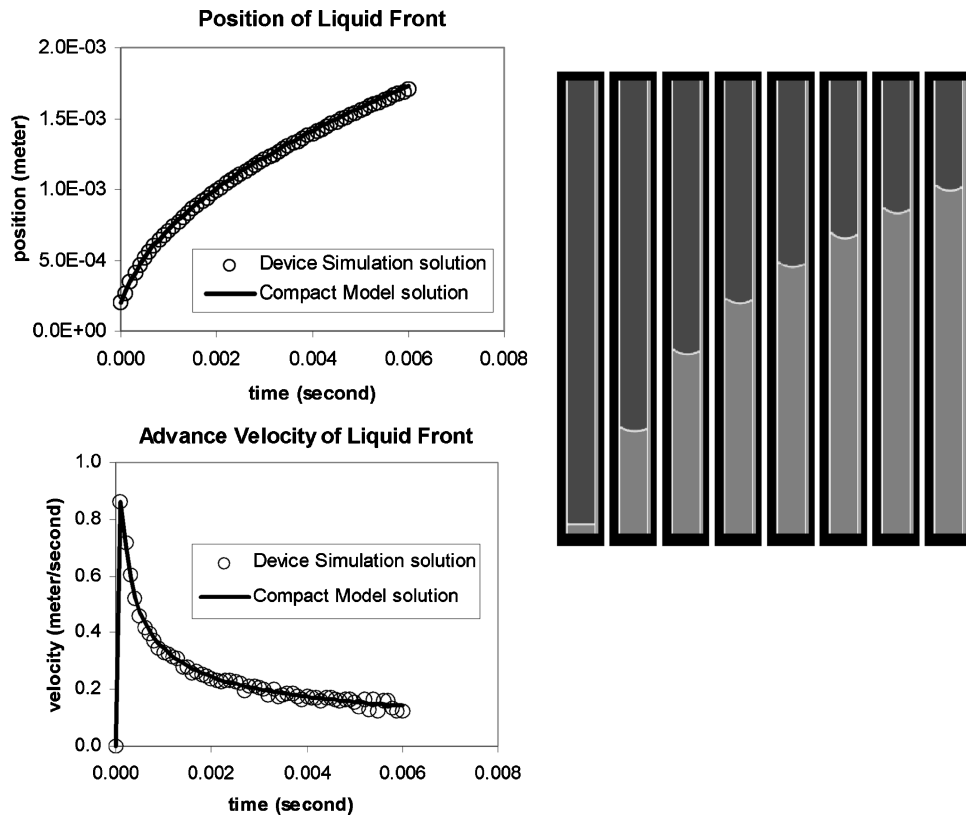


Fig. 8. Validation of the compact model derived from Eq. (4). Left shows the transient solutions of the liquid front position and its advance velocity. The device simulation solutions from Bubble-DropSim are plotted against the compact model solution and show excellent agreement. Right shows a sequence of the Bubble-DropSim solutions illustrating the transient capillary filling process.

Suppose that initially ( $t = 0$ ) the liquid holds column length of  $L_0$  and with zero velocity. The transient solution of this capillary-filling problem can be expressed as:

$$\begin{aligned} L &= \left[ -\frac{A}{B^2}(1 - \exp(-Bt)) + \frac{At}{B} + L_0^2 \right]^{1/2} \\ u &= \frac{A}{2BL}(1 - \exp(-Bt)) \end{aligned} \quad (4)$$

Equation (4) can be used directly to construct a compact model that simulates the capillary filling of a two-dimensional microchannel. Figure 8 shows the validation study of this compact model using Bubble-DropSim as the validation tool. The comparison shows an excellent match between the compact model and the capillary-filling process.

The analytical approach is one of primary methods to generate compact models for microfluidic devices. Illustrated above is an example of using an

analytical method to create a compact model for capillary filling in two-dimensional channel. The same underlying principle and similar procedures can be used to derive compact models for capillary filling inside more complex three-dimensional structures such as microrestrictors where the cross-section varies along the direction of the flow.

Figure 9 shows system simulation of capillary filling of a microfluidic subsystem. This subsystem integrates a liquid sample reservoir, a micropump driven by a piezoelectric-actuated monomorph diaphragm, a restrictor, a channel, a capillary gate, and a reaction chamber. This microfluidic subsystem is similar to the subsystems shown in Figures 4(a) and 4(b) where the capillary gates are implemented to stop the liquid stream. The CD-like device illustrated in Figure 4 uses centrifugal force (i.e., modulating the rotating speed) to break the capillary gate. Figure 9 illustrates via simulation the piezoelectric pumping effect that breaks the capillary gate.

Figure 9(a) shows the two-dimensional layout of this subsystem. This layout is then etched into glass and a three-dimensional device structure is formed, shown at the upper right corner of Figure 9(a) with the lid removed. Figure 9(b) shows the system schematic that is created by synthesizing the compact models. The labeling indicates the mapping between the compact models in Figure 9(b) and the devices in Figure 9(a). Initially the liquid resides only in the liquid sample reservoir. The surface tension force drives the liquid into the restrictor, and then the channel, and then stops at the capillary gate. Figures 9(c) and 9(d) show the simulation of this passive capillary filling and capillary gating process. Figure 9(c) shows the liquid length (nondimensionalized) inside various devices, and shows that only after the device at upper stream is completely filled, is the device at lower stream started to be filled. The flow rate becomes zero when the liquid front reaches the capillary gate. Figure 9(d) illustrates the dynamic contact angle phenomenon at the capillary gate that is responsible for stopping the liquid flow. The simulation shows that it takes a little more than 2 milliseconds to complete the capillary filling and gating processes.

After the capillary filling and gating are complete, at a desired time (at time equal to 4 milliseconds in this simulation), a voltage pulse is applied to the piezoelectric diaphragm and the deflection of the diaphragm generates flow, shown in Figure 9(e). Figure 9(f) shows that such flow breaks the capillary gate and the liquid starts to fill the device downstream.

## 6. SYNTHESIS METHODS

In this section, we provide an overview of the biochip synthesis, test, and reconfiguration techniques that have recently been published in the literature.

### 6.1 Synthesis and Reconfiguration Techniques

Architectural-level synthesis (i.e., high-level synthesis) was decoupled from geometry-level synthesis (i.e., physical design) in Su and Chakrabarty [2004, 2005a]. Architectural-level synthesis for microfluidic biochips can be viewed as the problem of scheduling assay functions and binding them to a given number of resources so as to maximize parallelism, thereby decreasing response

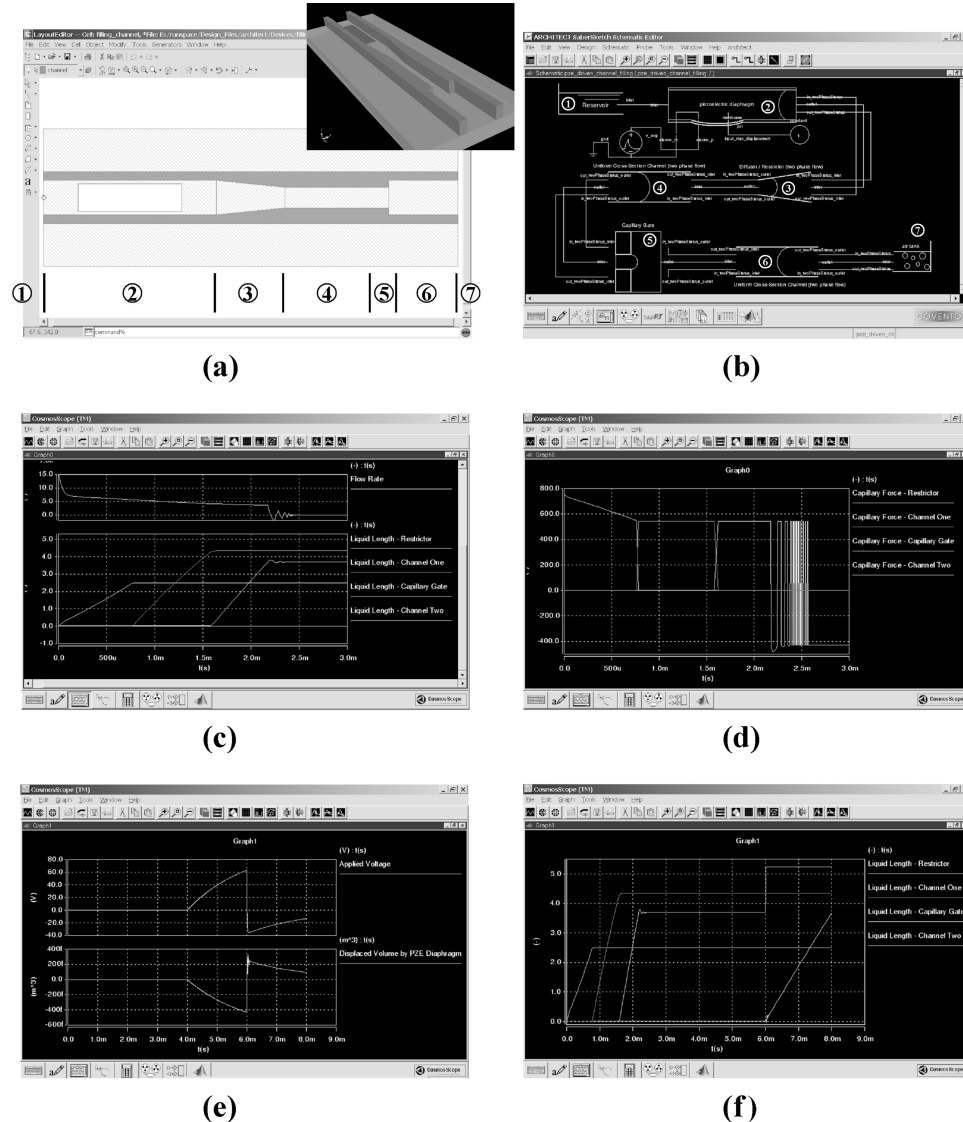


Fig. 9. System synthesis and simulation of liquid flow actuation and control of a microfluidic subsystem. (a) shows the two-dimensional layout of the subsystem. This subsystem is composed of seven devices. In the order of the labeling, they are liquid reservoir, chamber with a piezoelectric driven diaphragm mounted underneath, restrictor, channel one, capillary gate, channel two which links with an air source. A three-dimensional solid model of this subsystem is shown at the upper right corner. (b) shows the system schematic of this subsystem. The labeling for the synthesized compact models corresponds to the labeling in (a). (c) and (d) show the simulation of the passive capillary filling process. The flow rate in (c) shows the capillary gating action. The surface tension plot in (d) shows the dynamic contact angle effect. (e) and (f) show the simulation of the piezoelectric actuation and the break-up of the capillary gate. (e) shows the applied electric voltage and the displaced liquid volume. (f) shows that the capillary gate is broken and liquid starts to flow into channel two.

time. On the other hand, geometry-level synthesis addresses the placement of resources and the routing of droplets to satisfy objectives such as area or throughput. Defect/fault tolerance can also be included as a critical objective in the proposed synthesis method.

As in the case of high-level synthesis for integrated circuits, resource binding in the biochip synthesis flow refers to the mapping from bioassay operations to available functional resources. Note that there may be several types of resources for any given bioassay operation. For example, a  $2 \times 2$ -array mixer, a  $2 \times 3$ -array mixer and a  $2 \times 4$ -array mixer can be used for a droplet mixing operation, but with different mixing times. In such cases, a resource selection procedure must be used. On the other hand, resource binding may associate one functional resource with several assay operations; this necessitates resource sharing. Once resource binding is carried out, the time duration for each bioassay operation can be easily determined. Scheduling determines the start times and stop times of all assay operations, subject to the precedence and resource-sharing constraints. An optimal strategy based on integer linear programming has been developed for scheduling assay operations under resource constraints [Su and Chakrabarty 2004]. Since the scheduling problem is NP-complete, heuristic techniques for large problem instances have also been developed.

A key problem in the geometry-level synthesis of biochips is the placement of microfluidic modules such as different types of mixers and storage units. Since digital microfluidics-based biochips enable dynamic reconfiguration of the microfluidic array during run-time, they allow the placement of different modules on the same location during different time intervals. A simulated annealing-based heuristic approach has been developed to solve the NP-complete placement problem in a computationally efficient manner [Su and Chakrabarty 2005a]. Solutions for the placement problem can provide the designer with guidelines on the size of the array to be manufactured. If module placement is carried out for a fabricated array, area minimization frees up more unit cells for sample collection and preparation.

A synthesis methodology that unifies operation scheduling, resource binding, and module placement has also been developed [Su and Chakrabarty 2005b]; see Figure 10. Exact placement information, instead of a crude area estimate, is used to judge the quality of architectural-level synthesis. This method allows architectural design and physical design decisions to be made simultaneously. Moreover, fault tolerance can be easily incorporated during synthesis, whereby resources for assay functions are carefully selected and placed in the array to bypass defective cells; in this way, the assay functionality is not compromised. The requirement of real-time responsiveness in environmental sensing and clinical diagnostics applications motivates the need to minimize total assay analysis time. In order to increase sampling efficiency, we also attempt to free up more array area for sample collection and preparation by minimizing the area of the chip devoted to analysis.

Efficient reconfiguration techniques to bypass faulty unit cells in the microfluidic array have also been developed. A microfluidic module containing a faulty unit cell can easily be relocated to another part of the microfluidic

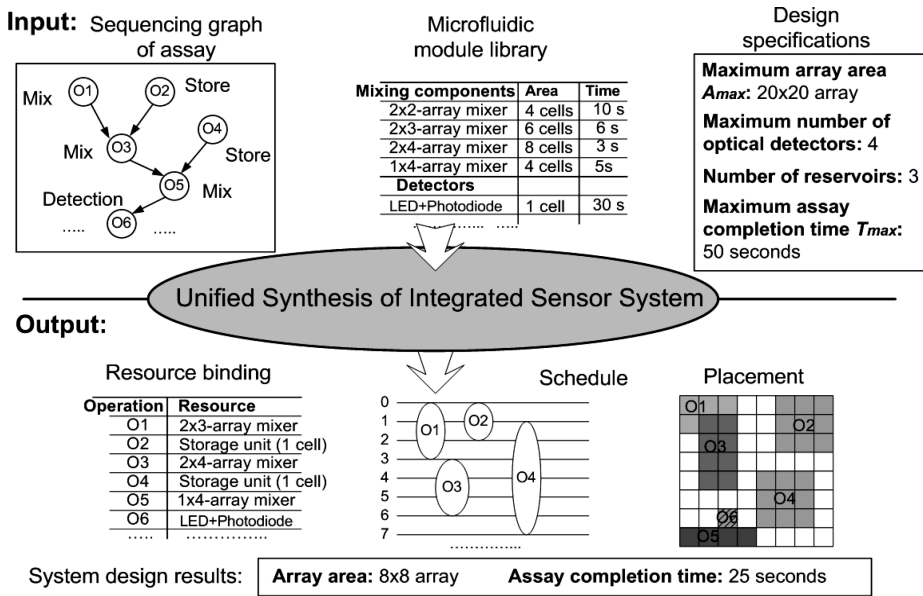


Fig. 10. An example illustrating unified synthesis.

array by changing the control voltages applied to the corresponding electrodes [Su and Chakrabarty 2005a]. Defect/fault tolerance can also be achieved by including redundant elements in the system; these elements can be used to replace faulty elements through reconfiguration techniques [Su et al. 2005a]. Another method is based on graceful degradation, in which all elements in the system are treated in a uniform manner, and no element is designated as a spare [Su and Chakrabarty 2005c]. In the presence of defects, a subsystem with no faulty element is first determined from the faulty system. This subsystem provides the desired functionality, but with a gracefully degraded level of performance (e.g., longer execution times). Due to the dynamic reconfigurability of digital microfluidics-based biochips, the microfluidic components (e.g., mixers) used during the bioassay can be viewed as reconfigurable virtual devices. For example, a  $2 \times 4$  array mixer (implemented using a rectangular array of control electrodes—two in the X-direction and four in Y-direction) can easily be reconfigured to a  $2 \times 3$  array mixer or a  $2 \times 2$  array mixer.

Figure 11 shows the module placement results and the microfluidic array design for a representative protein assay [Su and Chakrabarty 2005b]. Figure 11 shows the corresponding results when some of the unit cells in the array are faulty, and reconfiguration is used in a unified manner with synthesis. The solution obtained for the fault-free array yields a biochip design with a  $9 \times 9$  microfluidic array and the completion time for the protein assay is 363 seconds. The design for the faulty array allows the protein assay to operate with an increase of only 6% in the completion time, that is, the completion time is now 385 seconds.

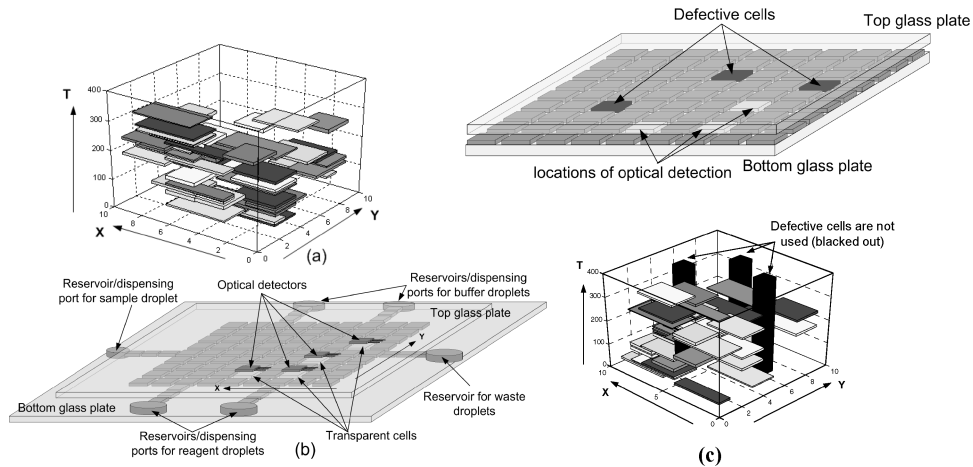


Fig. 11. (a) A 3-D model illustrating the synthesis results. (b) A digital microfluidic biochip for a protein assay. (c) A defective array and module placement for the protein assay on this array.

## 6.2 Testing Techniques and Design-For-Test (DFT)

The testing of MEMS, and bio-MEMS in particular, is still in its infancy. Recently, fault modeling and fault simulation in surface micromachined MEMS has received attention [ Kolpekwar and Blanton 1997; Deb and Blanton 2000]. Fault modeling, fault simulation, and a DFT methodology for continuous-flow microfluidic systems have also been proposed [Kerkhoff 1999; Kerkhoff and Hendriks 2001; Kerkhoff and Acar 2003 ]. Limited work on the testing of “digital” microfluidic biochips has been reported to date.

Faults in these systems have been classified as being either catastrophic or parametric [Jee and Ferguson 1993]. Catastrophic (hard) faults lead to a complete malfunction of the system, while parametric (soft) faults cause a deviation in the system performance. A parametric fault is detectable only if this deviation exceeds the tolerance in system performance.

Catastrophic faults in digital biochips may be caused by a number of physical defects, for example:

- Dielectric Breakdown*. The breakdown of the dielectric at high voltage levels creates a short between the droplet and the electrode. When this happens, the droplet undergoes electrolysis, thereby preventing further transportation.
- Short between the Adjacent Electrodes*. If a short occurs between two adjacent electrodes, the two electrodes effectively form one longer electrode. When a droplet resides on this electrode, it is no longer large enough to overlap the gap between adjacent electrodes. As a result, the actuation of the droplet can no longer be achieved.
- Degradation of the Insulator*. This degradation effect is unpredictable and may become apparent gradually during the operation of the microfluidic system. A consequence is that droplets often fragment and their motion is prevented because of the unwanted variation of surface tension forces along their flow path.

—*Open in the Metal connection between the Electrode and the Control Source.*  
 This defect results in a failure in activating the electrode for transport.

Physical defects that cause parametric faults include the following:

- Geometrical Parameter Deviation.* The deviation in insulator thickness, electrode length and height between parallel plates may exceed their tolerance value.
- Change in Viscosity of Droplet and Filler Medium.* These can occur during operation due to an unexpected biochemical reaction, or changes in operational environment, for example, temperature variation.

A unified test methodology for digital microfluidic biochips has been developed, whereby faults can be detected by controlling and tracking droplet motion electrically [Su et al. 2003, 2005b]. Test stimuli droplets containing a conductive fluid (e.g., KCL solution) are dispensed from the droplet source. These droplets are guided through the unit cells following the test plan towards the droplet sink, which is connected to an integrated capacitive detection circuit. Most catastrophic faults result in a complete cessation of droplet transportation [Su et al. 2003, 2005b]. Therefore, we can determine the fault-free or faulty status of the system by simply observing the arrival of test stimuli droplets at selected ports.

An efficient test plan not only ensures that testing does not conflict with the normal bioassay, but it also guides test stimuli droplets to cover all the unit cells available for testing. The test planning problem has been formulated in terms of the graph partitioning and the Hamiltonian path problems [Su et al. 2004a]. This method can be used for field-testing of digital microfluidics-based systems; as a result, it increases the system reliability during everyday operation [Su et al. 2004b]. With negligible hardware overhead, this method also offers an opportunity to implement self-test for microfluidic systems and therefore eliminate the need for costly, bulky, and expensive external test equipment. Furthermore, after detection, droplet flow paths for biomedical assays can be reconfigured dynamically such that faulty unit cells are bypassed without interrupting the normal operation.

## 7. CONCLUSIONS

We have provided an overview of presented several different actuation mechanisms for microfluidics-based biochips, as well as associated design automation trends and challenges in this emerging area. The underlying physical principles of electrokinetics, electrohydrodynamics, and thermocapillarity have been discussed. We have presented an integrated system-level design methodology that attempts to address key issues in the modeling, simulation, synthesis, testing and reconfiguration of digital microfluidics-based biochips. As microfluidics-based biochips gain popularity, and more chemical procedures and assays are executed concurrently on a biochip, system integration and design complexity are expected to increase dramatically. The top-down design automation flow presented here will facilitate the integration of fluidic components with micro-electronic component in next-generation SOCs.

## ACKNOWLEDGMENTS

The authors thank Fei Su of Duke University for help in preparing this article and for contributing to this work.

## REFERENCES

- ADAMSON, A. W. 1990. *Physical Chemistry of Surfaces*, 5th Ed. Wiley, New York.
- ANDERSON, J. D. 1995. *Computational Fluid Dynamics: The Basics with Applications*. McGraw-Hill, New York.
- AFFYMETRIX GENECHIP®. <http://www.affymetrix.com>.
- BATCHELOR, G. K. 2000. *An Introduction to Fluid Dynamics*. University Press, Cambridge, England.
- BREBBIA, C. A. 1978. *The Boundary Element Method for Engineers*. Pentech Press, London, England.
- BURNS, M. A., JOHNSON, B. N., BRAHMASANDRA, S. N., HANDIQUE, K., WEBSTER, J. R., KRISHNAN, M., SAMMARCO, T. S., MAN, P. M., JONES, D., HELDSINGER, D., MASTRANGELO, C. H., AND BURKE, D. T. 1998. An integrated nanoliter DNA analysis device. *Science* 282, 484–487.
- CHATTERJEE, A. N. AND ALURU, N. R. 2005. Combined circuit/device modeling and simulation of integrated microfluidic systems. *J. Microelect. Syst.* 14, 81–95.
- CHEN, J. Z., DARHUBER, A. A., TROIAN, S. M., AND WAGNER, S. 2004. Capacitive sensing of droplets for microfluidic devices based on thermocapillary actuation. *Lab on a Chip* 4, 473–480.
- CHO, S. K., FAN, S. K., MOON, H., AND KIM, C. J. 2002. Toward digital microfluidic circuits: Creating, transporting, cutting and merging liquid droplets by electrowetting-based actuation. In *Proceedings of IEEE MEMS Conference*. IEEE Computer Society Press, Los Alamitos, CA, 32–52.
- CHOI, C.-H., WESTIN, K. J. A., AND BRUER, K. S. 2003. Apparent slip flows in hydrophilic and hydrophobic microchannels. *Phys. Fluids* 15, 2897–2902.
- CLOUGH, R. W. 1960. The finite element method in plane stress analysis. In *Proceedings 2nd ASCE Conference on Electronic Computation* (Pittsburgh, PA). 345–378.
- COVENTORWARE™. <http://www.coventor.com>.
- DARHUBER, A. A., VALENTIN, J. P., TROIAN, S. M., AND WAGNER, S. 2003. Thermocapillary actuation of droplets on chemically patterned surfaces by programmable microheater arrays. *J. MicroElectroMechanical Syst.* 12, 873–879.
- DEB, N. AND BLANTON, R. D. 2000. Analysis of failure sources in surface-micromachined MEMS. In *Proceedings of International Test Conference*. 739–749.
- DUFFY, D. C., GILLIS, H. L., LIN, J., SHEPPARD, N. F., AND KELLOGG, G. J. 1999. Microfabricated centrifugal microfluidic systems: Characterization and multiple enzymatic assays. *Anal. Chem.* 71, 4669–4678.
- ERICKSON, D. 2005. Towards numerical prototyping of labs-on-chip, modeling for integrated microfluidic devices. *J. Microfluidics Nanofluidics*, 10.1007/s10404-005-0041-z.
- FITZPATRICK, D. AND MILLER, I. 1998. *Analog Behavioral Modeling with the Verilog—A Language*. Kluwer Academic Publishers, Boston, MA.
- GALLARDO, B. S., GUPTA, V. K., EAGERTON, F. D., JONG, L. I., CRAIG, V. S., SHAH, R. R., AND ABBOTT, N. L. 1999. Electrochemical principles for active control of liquids on submillimeter scales. *Science* 283, 57–60.
- GRAYSON, A., SHAWGO, R., JOHNSON, A., FLYNN, N., LI, Y., CIMA, M., AND LANGER, R. 2004. A bioMEMS review: MEMS technology for physiologically integrated devices. *Proc. IEEE* 92, 6–21.
- HARRISON, D. J., FLURI, K., SEILER, K., FAN, Z. H., EFFENHAUSER, C. S., AND MANZ, A. 1993. Micro-machining a miniaturized capillary electrophoresis-based chemical analysis system on a chip. *Science* 261, 895–897.
- HAUS, H. A. AND MELCHER, J. R. 1989. *Electromagnetic Fields and Energy*. Prentice-Hall, Englewood Cliffs, NJ.
- HIRSCH, C. 1988. *Numerical Computation of Internal and External Flows: Fundamentals of Numerical Discretization*. Wiley, New York.
- HIRT, C. W., AMSDEN, A. A., AND COOK, J. L. 1974. An Arbitrary Lagrangian-Eulerian computing method for all flow speeds. *J. Comput. Phys.* 14, 227–253.

- HIRT, C. W. AND NICHOLS, B. D. 1981. Volume of fluid (VOF) method for the dynamics of free boundaries. *J. Comput. Phys.* 39, 201–225.
- HOMSY, A., KOSTER, S., ELJKEL, J. C. T., VAN DEN BERG, A., LUCKLUM, F., VERPOORTE, E., AND DE ROOL, N. F. 2005. A high current density DC magnetohydrodynamic (MHD) micropump. *Lab on a Chip* 5, 466–471.
- HULL, H. F., DANILA, R., AND EHRESMANN, K. 2003. Smallpox and bioterrorism: Public-health responses. *J. Lab. Clin. Med.* 142, 221–228.
- ICHIMURA, K., OH, S., AND NAKAGAWA, M. 2000. Light-driven motion of liquids on a photoresponsive surface. *Science* 288, 1624–1626.
- INFINEON ELECTRONIC DNA CHIP. <http://www.infineon.com>.
- INTERNATIONAL TECHNOLOGY ROADMAP FOR SEMICONDUCTORS (ITRS). <http://public.itrs.net/Files/2003ITRS/Home2003.htm>.
- JACOBSON, S. C., HERGENRÖDER, R., KOUTNY, L. B., AND RAMSEY, J. M. 1994. High-speed separations on a microchip. *Anal. Chem.* 66, 1114–1118.
- JEE, A. AND FERGUSON, F. J. 1993. Carafe: An inductive fault analysis tool for CMOS VLSI circuits. In *Proceedings of IEEE VLSI Test Symposium*. IEEE Computer Society Press, Los Alamitos, CA, 92–98.
- JONES, T. B. 1973. Electrohydrodynamic heat pipes. *Int. J. Heat Mass Trans.* 16, 1045–1048.
- JONES, T. B. 2002. On the relationship of dielectrophoresis and electrowetting. *Langmuir* 18, 4437–4443.
- JONES, T. B., GUNJI, M., WASHIZU, M., AND FELDMAN, M. J. 2001. Dielectrophoretic liquid actuation and nanodroplet formation. *J. Appl. Phys.* 89, 1441–1448.
- KAHNG, A. B., MANDOUI, I., REDA, S., XU, X., AND ZELIKOVSKY, A. Z. 2003. Evaluation of placement techniques for DNA probe array layout. In *Proceedings of IEEE/ACM International Conference on Computer Aided Design*. ACM, New York, 262–269.
- KARNIADAKIS, G. AND BESKOK, A. 2001. *Microflows: Fundamentals and Simulation*. Springer-Verlag, Berlin, Germany.
- KERKHOFF, H. G. 1999. Testing philosophy behind the micro analysis system. In *Proceedings of SPIE: Design, Test and Microfabrication of MEMS and MOEMS* 3680, 78–83.
- KERKHOFF, H. G. AND ACAR, M. 2003. Testable design and testing of micro-electro-fluidic arrays. In *Proceedings of IEEE VLSI Test Symposium*. IEEE Computer Society Press, Los Alamitos, CA, 403–409.
- KERKHOFF, H. G. AND HENDRIKS, H. P. A. 2001. Fault modeling and fault simulation in mixed micro-fluidic microelectronic systems. *J. Elect. Testing: Theory Appl.* 17, 427–437.
- KOLPEKWAR, A. AND BLANTON, R. D. 1997. Development of a MEMS testing methodology. In *Proceedings of International Test Conference*, 923–931.
- LANDAU, L. D. AND LIFSHITZ, E. M. 1960. *Electrodynamics of Continuous Media*, Addison-Wesley, Reading, MA.
- LASER, R. D. J. AND SANTIAGO, J. G. 2004. A review of micropumps. *J. Micromech. Microeng.* 14, R35–R64.
- LAUGA, E. AND STONE, H. A. 2003. Effective slip in pressure-driven Stokes flow. *J. Fluid Mech.* 489, 55–77.
- LEAL, L. G. 1992. *Laminar Flow and Convective Transport Processes: Scaling Principles and Asymptotic Analysis*. Butterworth-Heinemann, Boston, MA.
- LION, N., ROHNER, T. C., DAYON, L., ARANUD, I. L., DAMOC, E., YOUEHOVSKI, I. N., WU, Z., ROUSSEL, C., JOSSERAND, J., JENSEN, H., ROSSIER, J., PRZYBLSKI, M., AND GIRAUT, H. 2003. Microfluidic systems in proteomics. *Electrophoresis* 24, 3533–3562.
- MACCORMACK, R. W. AND PAULLAY, A. J. 1972. Computational efficiency achieved by time splitting of finite difference operators. AIAA Paper, 72–154.
- MANTOTH, H. A. AND GIEGENBAUM, M. 1995. *Modeling with an Analog Hardware Description Language*. Kluwer Academic Publishers, Boston, MA.
- MANZ, A., HARRISON, D. J., VERPOORTE, E. M. J., FETTINGER, J. C., PAULUS, A., LUDI, H., AND WIDMER, H. M. 1992. Planar chips technology for miniaturization and integration of separation techniques into monitoring systems—Capillary electrophoresis on a chip. *J. Chromatogr.* 593, 253–258.
- MCDONALD, P. W. 1971. The computation of transonic flow through two-dimensional gas turbine cascades. ASME Paper 71-GT-89.

- MAXWELL, J. C. 1879. On stresses in rarified gases arising from inequalities of temperature. *Phil. Trans. R. Soc. Lond.* 170, 231–256.
- MELCHER, J. R. AND TAYLOR, G. I. 1969. Electrohydrodynamics: a review of the role of interfacial shear stresses. *Ann. Rev. Fluid Mech.* 1, 111–146.
- MELCHER, J. R. 1981. *Continuum Electromechanics*, Section 3.7, The MIT Press, Boston, MA.
- MUTLU, S., SVEC, F., MASTRANGELO, C. H., FRETCHT, J. M. J., AND GIANCHANDANI, Y. B. 2004. Enhanced electro-osmosis pumping with liquid bridge and field effect flow rectification. In *Proceedings of IEEE MEMS Conference*. 850–853.
- NANOGEN NANOCHIP®. <http://www.nanogen.com>.
- NAVIER, C. L. M. H. 1823. Mémoire sur les lois du mouvement des fluides. *Mémoires de l'Académie Royale des Sciences de l'Institut de France* 6, 389–440.
- NGUYEN, N.-T. AND HUANG, X. 2005. Thermocapillary effect of a liquid plug in transient temperature fields. *Japan. J. Appl. Phys.* 44, 1139–1142.
- PAIK, P., PAMULA, V. K., AND FAIR, R. B. 2003. Rapid droplet mixers for digital microfluidic systems. *Lab on a Chip* 3, 253–259.
- PAN, F., KUBBY, J., AND CHEN, J. 2002. Numerical simulation of fluid-structure interaction in a MEMS diaphragm drop ejector. *J. Micromech. Microeng.* 12, 70–76.
- POHL, H. A. 1978. *Dielectrophoresis: The Behaviour of Neutral Matter in Nonuniform Electric Fields*, Cambridge University Press, Cambridge, England.
- POLLACK, M. G. 2001. *Electrowetting-Based Microactuation of Droplets for Digital Microfluidics*. Ph.D. dissertation. Duke University.
- POLLACK, M. G., FAIR, R. B., AND SHENDEROV, A. D. 2000. Electrowetting-based actuation of liquid droplets for microfluidic applications. *Appl. Phys. Lett.* 77, 1725–1726.
- POLLACK, M. G., SHENDEROV, A. D., AND FAIR, R. B. 2002. Electrowetting-based actuation of droplets for integrated microfluidics. *Lab on a Chip* 2, 96–101.
- PRINS, M. W. J., WELTERS, W. J. J., AND WEEKAMP, J. W. 2001. Fluid control in multichannel structures by electrocapillary pressure. *Science* 291, 277–280.
- PROBSTEIN, R. F. 1994. *Physicochemical hydrodynamics*. Wiley, New York.
- RUDNYI, E. B. AND KORVINK, J. G. 2002. Review: Automatic Model Reduction for Transient Simulation of MEMS-based Devices. *Sensors Update* 11, 3–33.
- SAMMARCO, T. S. AND BURNS, M. A. 1999. Thermocapillary pumping of discrete droplets in micro-fabricated analysis devices. *AI Che J.* 45, 350–366.
- SAVILLE, D. A. 1977. Electrokinetic effects with small particles. *Ann. Rev. Fluid Mech.* 9, 321–337.
- SCHULTE, T. H., BARDELL, R. L., AND WEIGL, B. H. 2002. Microfluidic technologies in clinical diagnostics. *Clinica Chimica Acta* 321, 1–10.
- SCHWARTZ, J. A., VYKOUKAL, J. V., AND GASCOYNE, P. R. C. 2004. Droplet-based chemistry on a programmable micro-chip. *Lab on a Chip* 4, 11–17.
- SENTURIA, S. D. 1998. CAD challenges for microsensors, microactuators, and microsystems. *Proc. IEEE* 86, 1611–1626.
- SHAPIRO, B., MOON, H., GARRELL I. R., AND KIM, C. J. 2003. Modeling of electrowetted surface tension for addressable microfluidic systems: Dominant physical effects, material dependences, and limiting phenomena. In *Proceedings of IEEE MEMS Conference*. IEEE Computer Society Press, Los Alamitos, CA, 201–205.
- SMITS, J. G. 1990. Piezoelectric micropump with three valves working peristaltically. *Sensors and Actuators A* 21, 304–306.
- SRINIVASAN, V. 2005. *A Digital Microfluidic Lab-on-a-Chip for Clinical Diagnostic Applications*, Ph.D. dissertation. Duke University.
- SRINIVASAN, V., PAMULA, V. K., AND FAIR, R. B. 2004. An integrated digital microfluidic lab-on-a-chip for clinical diagnostics on human physiological fluids. *Lab on a Chip* 4, 310–315.
- SRINIVASAN, V., PAMULA, V. K., POLLACK, M. G., AND FAIR, R. B. 2003a. A digital microfluidic biosensor for multianalyte detection. In *Proceedings of IEEE MEMS Conference*. IEEE Computer Society Press, Los Alamitos, CA, 327–330.
- SRINIVASAN, V., PAMULA, V. K., POLLACK, M. G., AND FAIR, R. B. 2003b. Clinical diagnostics on human whole blood, plasma, serum, urine, saliva, sweat, and tears on a digital microfluidic platform. In *Proceedings of Micro Total Analysis Systems*, 1287–1290.

- STONE, H. A., STROOCK, A. D., AND AIDARI, A. 2004. Engineering flows in small devices: microfluidics toward a lab-on-a-chip. *Ann. Rev. Fluid Mech.* 36, 381–411.
- SU, F. AND CHAKRABARTY, K. 2004. Architectural-level synthesis of digital microfluidics-based biochips. In *Proceedings of IEEE/ACM International Conference on Computer Aided Design*. IEEE Computer Society Press, Los Alamitos, CA, 223–228.
- SU, F. AND CHAKRABARTY, K. 2005a. Design of fault-tolerant and dynamically-reconfigurable microfluidic biochips. In *Proceedings of Design, Automation and Test in Europe (DATE) Conference*. 1202–1207.
- SU, F. AND CHAKRABARTY, K. 2005b. Unified high-level synthesis and module placement for defect-tolerant microfluidic biochips. In *Proceedings of IEEE/ACM Design Automation Conference*, ACM, New York, 825–830.
- SU, F. AND CHAKRABARTY, K. 2005c. Defect tolerance for gracefully-degradable microfluidics-based biochips. In *Proceedings of IEEE VLSI Test Symposium*. IEEE Computer Society Press, Los Alamitos, CA, 321–326.
- SU, F., CHAKRABARTY, K., AND PAMULA, V. K. 2005a. Yield enhancement of digital microfluidics-based biochips using space and local reconfiguration. In *Proceedings of Design, Automation and Test in Europe (DATE) Conference*. 1196–1201.
- SU, F., OZEV, S., AND CHAKRABARTY, K. 2003. Testing of droplet-based microelectrofluidic systems. In *Proceedings of IEEE International Test Conference*. IEEE Computer Society Press, Los Alamitos, CA, 1192–1200.
- SU, F., OZEV, S., AND CHAKRABARTY, K. 2004a. Test planning and test resource optimization for droplet-based microfluidic systems. In *Proceedings of European Test Symposium*. 72–77.
- SU, F., OZEV, S. AND CHAKRABARTY, K. 2004b. Concurrent testing of droplet-based microfluidic systems for multiplexed biomedical assays. In *Proceedings of IEEE International Test Conference*. IEEE Computer Society Press, Los Alamitos, CA, 883–892.
- SU, F., OZEV, S. AND CHAKRABARTY, K. 2005b. Ensuring the operational health of droplet-based microelectrofluidic biosensor systems. *IEEE Sensors J.* 5, 763–773.
- SWART, N. R., BART, S. F., ZAMAN, M. H., MARIAPPAN, M., GILBERT, J. R., AND MURPHY, D. 1998. AutoMM: Automatic generation of dynamic macromodels for MEMS devices. In *Proceedings of 11th IEEE International Workshop on Micro Electromechanical Systems* (Heidelberg, Germany). IEEE Computer Society Press, Los Alamitos, CA, 178–183.
- TEZDUYAR, T. E., BEHR, M., MITTAL, S., AND LIOU, J. 1992a. New strategy for finite element computations involving moving boundaries and interfaces. The deforming-spatial-domain/space-time procedure. I. The concept and the preliminary numerical tests, *Comput. Meth. Appl. Mech. Eng.* 94, 339–351.
- TEZDUYAR, T. E., BEHR, M., MITTAL, S., AND LIOU, J. 1992b. New strategy for finite element computations involving moving boundaries and interfaces. The deforming-spatial-domain/space-time procedure. II. Computation of free-surface flows, two-liquid flows, and flows with drifting cylinders. *Comput. Meth. Appl. Mech. Eng.* 94, 353–371.
- THOMPSON, J. F. 1984. A survey of grid generation techniques in computational fluid dynamics. *AIAA J.* 22, 1505–1523.
- THORSEN, T., MAERKL, S., AND QUAKE, S. 2002. Microfluidic large-scale integration. *Science* 298, 580–584.
- TSENG, Y.-T., TSENG, F.-G., CHEN, Y.-F. AND CHIENG, C.-C. 2004. Fundamental studies on micro-droplet movement by Marangoni and capillary effects. *Sensors and Actuators A: Physical* 114, 292–301.
- TURNER, M. J., CLOUGH, R. W., MARTIN, H. C., AND TOPP, L. P. 1956. Stiffness and deflection analysis of complex structures. *J. Aeronaut. Sci.* 23, 805–824.
- TUROWSKI, M., CHEN, Z., AND PRZEKwas, A. 2001. Automated generation of compact models for fluidic microsystems. *Anal. Integ. Circuits Signal Proc.* 29, 27–36.
- VALENTINO, J. P., TROIAN, S. M., AND WAGNER, S. 2005. Microfluidic detection and analysis by integration of thermocapillary actuation with a thin-film optical waveguide. *Appl. Phys. Letters* 86, 184101:1–3.
- VENKATESH, S. AND MEMISH, Z. A. 2003. Bioterrorism: a new challenge for public health. *Int. J. Antimicro. Agents* 21, 200–206.

- VERHEIJEN, H. J. J. AND PRINS, M. W. J. 1999. Reversible electrowetting and trapping of charge: Model and experiments. *Langmuir* 15, 6616–6620.
- VERPOORTE, E. AND DE ROOI, N. F. 2003. Microfluidics meets MEMS. *Proc. IEEE* 91, 930–953.
- VYKOUKAL, J., SCHWARTZ, J. A., BECKER, F. F., AND GASCOYNE, P. R. C. 2001. A programmable dielectric fluid processor for droplet-based chemistry. In *Proceedings of Micro Total Analysis Systems*. 72–74.
- WANG, Y., LIN, Q., AND MUKHERJEE, T. 2005a. Composable behavioral models and schematic-based simulation of electrokinetic lab-on-a-chip. Accepted for publication in *IEEE Trans. CAD*.
- WANG, Y., LIN, Q., AND MUKHERJEE, T. 2005b. A model for laminar diffusion-based complex electrokinetic passive micromixers. *Lab On a Chip* 5, 877–887.
- WASHIZU, M. 1998. Electrostatic actuation of liquid droplets for microreactor applications. *IEEE Trans. Industry Appl.* 34, 732–737.
- WIXFORTH, A. AND SCRIBA, J. 2002. Nanopumps for programmable biochips. GIT Labor-Fachzeitschrift (May), pp. 231–232, (See also <http://www.advalytics.de>.)
- XIE, J., SHIH, J., LIN, Q., YANG, B., AND TAI, Y.-C. 2004. Surface micromachined electrostatically actuated micro peristaltic pump. *Lab on a Chip* 4, 495–501.
- ZENG, J., BANERJEE, D., DESHPANDE, M., GILBERT, J., DUFFY, D., AND KELLOGG, G. 2000. Design analyses of capillary burst valves in centrifugal microfluidics. In *Micro Total Analysis Systems*, Kluwer Academic Publishers, Enschede, The Netherlands, 579–582.
- ZENG, S., CHEN, C.-H., MIKKELSON, J. C., AND SANTIAGO, J. G. 2001. Fabrication and characterization of electroosmotic micropumps. *Sens. Act. B (Chemical)* 79, 107–114.
- ZENG, J. AND KORMSMAYER, F. T. 2004. Principles of droplet electrohydrodynamics for lab-on-a-chip. *Lab on a Chip* 4, 265–277.
- ZHANG, T., CHAKRABARTY, K., AND FAIR, R. B. 2002. *Microelectrofluidic Systems: Modeling and Simulation*, CRC Press, Boca Raton, FL.
- ZOVAL, J. V. AND MADOU, M. J. 2004. Centrifuge-based fluidic platforms. *Proc. IEEE* 92, 140–153.

Received October 2005; revised December 2005; accepted December 2005